Palaeogeography, Palaeoclimatology, Palaeoecology 516 (2019) 244–267

Contents lists available at ScienceDirect

Palaeogeography, Palaeoclimatology, Palaeoecology

journal homepage: www.elsevier.com/locate/palaeo

Revisiting the equable climate problem during the Late Cretaceous greenhouse using paleosol carbonate clumped isotope temperatures from the Campanian of the Western Interior Basin, USA

Landon Burgener[a,b,*], Ethan Hyland[b], Katharine W. Huntington[a], Julia R. Kelson[a], Jacob O. Sewall[c]

[a] Department of Earth and Space Sciences, University of Washington, Seattle, WA, United States
[b] Department of Marine, Earth, and Atmospheric Sciences, North Carolina State University, Raleigh, NC, United States
[c] Department of Physical Sciences, Kutztown University of Pennsylvania, Kutztown, PA, United States

ARTICLE INFO

Keywords:
Seasonality
Stable isotopes
Terrestrial paleoclimatology
Equability
Historical biogeography
Dinosaur provincialism

ABSTRACT

Greenhouse climates such as the Late Cretaceous period provide important reference frames for understanding modern anthropogenic climate change. Upper Cretaceous terrestrial climate proxies have been interpreted as evidence for "equable" climates with reduced seasonal variations in temperature. However, climate models have largely failed to reproduce these reconstructions unless parameters such as atmospheric CO_2 concentrations are set to unreasonable values. To help resolve such model-proxy disagreements, we reconstruct mean annual range in temperature (MART) for the Campanian (~75 Ma) Kaiparowits (south-central Utah) and Two Medicine (northwest Montana) Formations using warmest mean monthly temperature reconstructions from the clumped isotope composition of paleosol carbonate nodules, and reconstructions of local mean annual air temperatures from other methods. An evaluation of the applicability of bulk elemental soil geochemistry temperature proxies in these deposits supports the use of previous leaf physiognomy-based estimates of mean annual temperature for our MART reconstructions. We test the validity of several common assumptions made in reconstructing MART in two novel ways. First, MART is commonly calculated as twice the difference between local mean annual air temperature and warmest mean monthly temperature, and we validate this method by estimating modern MART for a range of environments using climate reanalysis data. Second, we constrain the effect of radiative soil heating on our soil carbonate temperature estimates by showing that for most environments likely to be preserved in the geologic record, summer soil temperatures are $< 3\,^{\circ}C$ higher than air temperatures. Our findings suggest that warmest mean monthly temperatures were 30 to 35 $\pm$ 4 °C at the two study sites, and that MART was 21 to 29 °C for the Kaiparowits Formation, and 21 to 27 °C for the Two Medicine Formation. Mid-latitude Late Cretaceous MARTs were similar to modern ranges in mid-latitude seasonal temperature, and much ($> 9\,^{\circ}C$) larger than previous proxy reconstructions of Late Cretaceous MART. These results add to a growing body of literature showing that terrestrial MART during ancient greenhouse periods was not significantly different from modern seasonal temperature variations. Finally, the similarity in MART between the Kaiparowits and Two Medicine formations suggests that latitudinal changes in MART did not contribute to the faunal provincialism that has been proposed by some paleontologists.

1. Introduction

Periods of elevated earth surface temperatures (e.g., greenhouse episodes) like the Late Cretaceous are natural laboratories for studying how the Earth's climate system behaves under elevated atmospheric CO_2 concentrations. However, our understanding of terrestrial climate conditions during these greenhouse periods is hampered by long-standing disagreement between proxy reconstructions and model simulations (e.g., Donnadieu et al., 2006; Huber, 2008; Sloan and Morrill, 1998; Sloan and Barron, 1990; Barron, 1987 and 1983). One of the most well-known of these proxy-model discrepancies is the inability of climate models to simulate the mean annual range of temperature (MART) evidenced by terrestrial proxy records, which show above-freezing winter temperatures and warm mean annual temperatures at

* Corresponding author at: Department of Earth and Space Sciences, University of Washington, Seattle, WA, United States.
E-mail address: lkb57@uw.edu (L. Burgener).

https://doi.org/10.1016/j.palaeo.2018.12.004
Received 24 August 2018; Received in revised form 6 December 2018; Accepted 6 December 2018
Available online 10 December 2018
0031-0182/

mid- to high-latitudes during the Late Cretaceous and Early Paleogene (Upchurch et al., 2015). This issue is a key component of the "equable climate problem", and is considered a classic unsolved question in paleoclimatology (Huber and Caballero, 2011; Spicer et al., 2008; DeConto et al., 2000). Additionally, beyond resolving the disagreement between proxy reconstructions and model simulations of MART, characterizing changes to MART during different climate states is also of interest because 1) the ancient and modern biogeography of many plants and animals (e.g., palms [Reichgelt et al., 2018] and crocodiles [Markwick, 1998]) are controlled by seasonal temperatures; and 2) characterization of MART during greenhouse periods may also provide insight into how temperature seasonality may evolve under future scenarios of human-induced climate change.

The Campanian (~75 Ma) sedimentary record of western North America is an exceptional continental-scale record of climatic, geologic, and biologic changes during the Late Cretaceous, and provides an opportunity to constrain MART during a greenhouse period. The western margin of the Western Interior Seaway contains numerous well-dated and correlated formations that contain abundant carbonate-bearing paleosols (e.g., Foreman et al., 2015, 2011; Roberts, 2007; Nordt et al., 2006; Rogers, 1995). These carbonate-bearing paleosols are an archive of changing paleoclimate conditions, and can provide quantitative reconstructions of key climate parameters such as Earth-surface temperature and mean annual precipitation (Sheldon and Tabor, 2009). Importantly, these formations also contain an extensive, intensively studied fossil record (Gates et al., 2010), making it possible to not only reconstruct Late Cretaceous paleoclimate conditions, but to examine the impact of climate parameters like MART on the evolution and distribution of terrestrial flora and fauna.

The main objective of this study is to revisit the question of seasonal equability in greenhouse climates and to place new constraints on MART during the Late Cretaceous by using carbonate clumped isotope paleothermometry of pedogenic (formed in soil) carbonate nodules. Specifically, we reconstruct warmest mean monthly soil and air temperatures using paleosols from two Campanian (~75 Ma) sedimentary deposits along the western margin of the Western Interior Seaway (WIS): the Kaiparowits Formation (KF), which crops out in modern south-central Utah, USA, and the Two Medicine Formation (TMF), in modern northwestern Montana, USA. We present new MAT and MAP estimates based on the paleo-weathering index (PWI) and chemical index of alteration without potassium (CIA−K) bulk geochemistry proxies, which we evaluate in the context of paleosol characteristics and previous quantitative reconstructions based on leaf margin analysis (LMA), CLAMP, and vertebrate phosphate $\delta^{18}O$. These comparisons establish that the PWI and CIA-K methods are not appropriate for the KF and TMF paleosols, and that leaf physiognomy and vertebrate phosphate $\delta^{18}O$ proxies provide more reasonable estimates of MAAT for the KF and TMF. Our new Δ_{47}-based reconstructed summer estimates and these previous MAAT reconstructions are paired to calculate MART based on the assumption that the annual distribution of air temperatures is symmetrical about the MAAT. In addition to providing new constraints on climate in western North America during the Late Cretaceous, we examine the errors and uncertainties associated with several common assumptions made when calculating summer air temperatures and MART with clumped isotope data. Taken together, our results provide a framework for more accurate estimates of paleo-MART during greenhouse periods, and more reliable climate interpretations of paleosol carbonates. Our MART reconstructions for the Late Cretaceous expand the available estimates of seasonality during greenhouse periods, providing a new point of comparison for similar work in the Paleocene and Eocene (e.g. Hyland et al., 2018; Snell et al., 2013).

2. Background

2.1. Global and North American climate during the Late Cretaceous

Previous proxy reconstructions have characterized Late Cretaceous global climate as warm and highly equable, with a reduced latitudinal temperature gradient and—of particular interest with respect to this study—reduced MART. Globally averaged mean annual air temperature (MAAT) was 6 to 14 °C warmer during the Late Cretaceous than the modern (Niezgodzki et al., 2017; DeConto et al., 1999; Barron et al., 1995). Proxy reconstructions of terrestrial latitudinal temperature gradients during the Campanian and Maastrichtian (latest Cretaceous) range from 0.3 to 0.4 °C °latitude^{-1} (Upchurch et al., 2015; Amiot et al., 2004; Wolfe and Upchurch, 1987) and are much lower than the modern temperature gradient (~0.6 to 1.0 °C °latitude^{-1}; Hay, 2008; Greenwood and Wing, 1995). Quantitative estimates of Late Cretaceous MART are scarce, but suggest reduced MART (Hunter et al., 2013; Wolfe and Upchurch, 1987).

In western North America, numerous studies have presented paleotemperature reconstructions during the Campanian. Some of these studies have focused on specific formations (e.g., Miller et al., 2013; Nordt et al., 2011; Nordt et al., 2003), and others focused on regional paleoclimate/latitudinal temperature trends (e.g., Wolfe and Upchurch, 1987). Miller et al. (2013) reported a MAAT of 20 ± 2 °C for the KF based on leaf-margin analysis (LMA), and Wolf and Upchurch (1987) estimated a MAAT of 16 ± 4 °C for the TMF based on reconstructions from the climate leaf analysis multivariate program (CLAMP). Additionally, Snell et al. (2014) reported three carbonate clumped isotope temperatures for the TMF (two lacustrine samples and one paleosol nodule) ranging from 29 to 32 °C. After accounting for a Late Cretaceous latitudinal temperature gradient of 0.3 to 0.4 °C °latitude^{-1}, temperature reconstructions from other coeval formations in relatively close proximity to the KF and TMF suggest that MAAT was between 17 and 21 °C for the KF (Upchurch et al., 2015; Miller et al., 2013; Wolfe, 1990), and 14 to 19 °C for the TMF (Barrick et al., 1999; Van Boskirk, 1998; Wolfe and Upchurch, 1987).

Precipitation rates are notoriously difficult to constrain, but some quantitative and qualitative proxy and model mean annual precipitation estimates for Late Cretaceous North America do exist. Based on the distribution of leaf sizes from multiple North American fossil leaf assemblages, precipitation appears to have been fairly constant throughout the year below paleolatitude ~40 °N, but more seasonal at higher latitudes (Falcon-Lang, 2003; Wolfe and Upchurch, 1987). No quantitative estimates of MAP exist for the TMF; however, studies using evidence from Maastrichtian paleosols in Montana suggest that Late Cretaceous MAP was 900–1200 mm yr^{-1} at ~49 °N (Falcon-Lang, 2003; Retallack, 1994). Miller et al. (2013) estimated MAP to be 1780 mm yr^{-1} (1240 to 2550 mm yr^{-1}) for the KF based on the leaf size distribution of multiple KF fossil leaf assemblages. Falcon-Lang (2003) showed that the TMF likely experienced large seasonal changes in precipitation based on an analysis of growth interruptions in fossil trees, which is consistent with modeling work done by Fricke et al. (2010) and Sewall and Fricke (2013) suggesting that there was a significant seasonal (monsoonal) pattern to North American precipitation during the Late Cretaceous.

2.2. Estimating Late Cretaceous MART in North America

Available proxy reconstructions for North America during the Late Cretaceous suggest MART values that are significantly smaller than modern MART at similar latitudes. Early leaf physiognomy studies suggested that during the Late Cretaceous, MART in North America was just 8 °C at a paleolatitude of 52 to 55° N (Wolfe and Upchurch, 1987), and CLAMP analyses summarized by Hunter et al. (2013) (see Tables 2 and 3) suggest a similarly small North American MART (~10 °C). These MART estimates are comparable to the mean MART of 13.5 °C

reconstructed for Eocene North America (Greenwood and Wing, 1995), and much lower than the ~25 to 30 °C MART estimated for modern North America at 50 to 55° N from ERA-Interim climate reanalysis data (Dee et al., 2011). The low MARTs estimated for both the Late Cretaceous and Eocene have been interpreted as being consistent with semi-quantitative evidence for winter temperatures above 5 °C based on the presence of fossil crocodilians and palms at high latitudes during these time periods (Markwick, 1998; Greenwood and Wing, 1995).

However, these proxy-based reconstructions of an equable Late Cretaceous/Eocene climate clash with model simulations that fail to reproduce such low MARTs. For example, Spicer et al. (2008) presented a detailed proxy-model comparison of Late Cretaceous Siberian seasonal temperatures, reporting CLAMP-derived MAAT, coldest mean monthly air temperature, and warmest mean monthly temperature values of 13.1, 5.8, and 21.1 °C, respectively (MART = 15.3 °C). They found that model simulations using a range of orbital configurations, atmospheric CO_2 and CH_4 concentrations, oceanic heat transport schemes, and vegetation conditions produced significantly larger MART estimates (~55 °C). Similarly, Hunter et al. (2013) conducted a model-proxy comparison of North American Late Cretaceous temperatures and showed that their model simulations underestimated CLAMP coldest month mean air temperature reconstructions by up to 12 °C depending on model parameters.

The inability of climate models to reproduce equable MART during greenhouse periods has been attributed to issues with both proxy records and climate models (Huber, 2008; Deconto et al., 1999). For example, leaf physiognomy proxies (LMA, CLAMP, and digital leaf physiognomy) of MAAT must take into account non-climate factors that affect leaf physiognomy (Peppe et al., 2011; Kowalski and Dilcher, 2003; Gregory-Wodzicki, 2000), as well as (in the case of CLAMP) methodological issues (Royer, 2012). However, despite these challenges, the relationship between MAAT and leaf margin morphology has been shown to be robust and statistically significant across a range of geographic areas (Peppe et al., 2017; Royer, 2012). In contrast, leaf physiognomy reconstructions of coldest and warmest month temperatures suffer from all of the same challenges as MAAT reconstructions, and face additional problems as well. For example, coldest and warmest month temperatures are more likely to be regionally dependent than MAAT, and are susceptible to covariation (Peppe et al., 2011, 2010; Jordan et al., 1996, Jordan, 1997). With respect to paleoclimate model simulations, the proposed issues appear to be less well defined, but are thought to include: 1) limited model spatial and temporal resolution (Snell et al., 2013; Sewall and Sloan, 2006); 2) unrealistic or undefined land cover schemes (Thrasher and Sloan, 2010); and 3) inaccurate or poorly resolved boundary conditions (e.g., the presence of oceanic gateways; Hunter et al., 2013; Donnadieu et al., 2006).

We provide new insight into this question of greenhouse seasonality by calculating Late Cretaceous MART as twice the difference between previous MAAT estimates and soil carbonate clumped isotope formation temperatures, following the methods of Snell et al. (2013). In addition to generating new estimates of Late Cretaceous MART, we provide important constraints on this method's accuracy by: 1) constraining the errors associated with calculating MART from just warmest month air or soil temperatures and MAAT; and 2) employing long term modern soil and air temperature datasets to estimate the typical range of radiative soil heating (ST_{RH}) caused by direct solar radiation, allowing for more accurate conversion of soil temperatures to air temperatures.

2.3. Geologic setting

The Upper Cretaceous non-marine sedimentary rocks of the TMF and KF are part of a large, north-south trending clastic wedge that was deposited into the subsiding Cordilleran foreland basin (e.g., the Western Interior Basin) by eastward-flowing fluvial systems beginning in the middle Jurassic and extending through the Eocene (Fig. 1; Foreman et al., 2011; Roberts, 2007; Kauffman and Caldwell, 1993). This body of sedimentary rocks formed a broad alluvial and coastal plain between the fold-and-thrust belt and the western margin of the WIS that stretched from the southern United States into northern Canada. Broadly speaking, both the TMF and the KF represent alluvial plain depositional environments; however, the TMF was characterized by relatively lower sedimentation rates and a semi-arid environment (Rogers, 1995), while the KF is notable for having the highest calculated sedimentation rates of any Upper Cretaceous formation along the WIS, and is characterized by an extremely humid, wet environment (Roberts, 2007). We note that the similarity in depositional environments for the two sites, as well as their similar position on the margin of the WIS suggest that they formed at similar elevations. Evaluation of seasonality in these two distinct environments allows us to explore the sensitivity of our proxies to different pedotypes, and make robust MART estimates.

The TMF is composed of alluvial sediments that were deposited during two third-order regressive/transgressive cycles (R7-T8 and R8-T9) of the WIS (Foreman et al., 2011, 2008; Rogers, 1998). The formation is characterized by laterally extensive fluvial fine- to medium-grained sandstones (braided and meandering channel facies) that alternate with siltstone interfluvial facies characterized by well-developed paleosols and rare lacustrine units (Foreman et al., 2011; Rogers, 1998). The paleosols are relatively well developed and are characterized by meter scale red horizons that are typically mottled and contain root traces (Foreman et al., 2011). Numerous bentonitic ash layers are intercalated between the TMF paleosols. These bentonites were described and dated by Rogers et al. (1993) and Foreman et al. (2008), yielding $^{40}Ar/^{39}Ar$ ages ranging from 79.72 ± 0.03 Ma at 80 m above the base of the TMF, to 77.52 ± 0.03 Ma at 265 m above the base of the TMF. The latter age comes from a bentonite sample collected from the Hagan's Crossing locality measured and sampled as part of this study (Fig. 1).

The KF is characterized by freshwater and terrestrial depositional environments, as well as a minor section of tidally influenced environments (Roberts, 2007) that were deposited under high sediment accumulation rates (~40 cm ka^{-1} compared to ~7 cm ka^{-1} for the TMF). The KF paleosols are typically weakly developed, with drab gray colors, incipient horizon development, and various pedogenic features typical of hydromorphic soils (e.g., gleying, siderite/pyrite accumulations). Roberts (2007) classified most of the KF paleosols as early Entisols, with rare calcite-nodule-bearing Inceptisols suggestive of more prolonged pedogenic activity. These poorly developed paleosols are consistent with the high sedimentation rates, high water table, and overall humid conditions estimated for the KF. Age constraints for the KF come from four bentonite ash layers sampled by Roberts et al. (2005), which yielded $^{40}Ar/^{39}Ar$ ages ranging from 75.96 ± 0.02 Ma at 80 m above the base of the KF, to 74.21 ± 0.11 Ma at 790 m above the base of the KF.

3. Methods

3.1. Paleosol mapping and sampling methods

At both the KF and TMF sampling sites (Table 1), individual paleosols were identified and their depth profiles described based on pedogenic features such as horizonation, grain size, color, and clay accumulation, as well the as presence/absence of specific features such as carbonate nodules, mottling, root traces, and slickensides. Paleosols were characterized within the context of previously measured stratigraphic sections (see Roberts, 2005, for a detailed description of the KF stratigraphy and Rogers, 1995, for the TMF stratigraphy). Each paleosol profile was measured and described after trenching to expose fresh material and avoid modern sediment and soil contamination. Paleosol types were classified based on the descriptive schemes of Mack et al. (1993) and Retallack et al. (1993). Where present, multiple carbonate nodules were collected to ensure adequate characterization of the

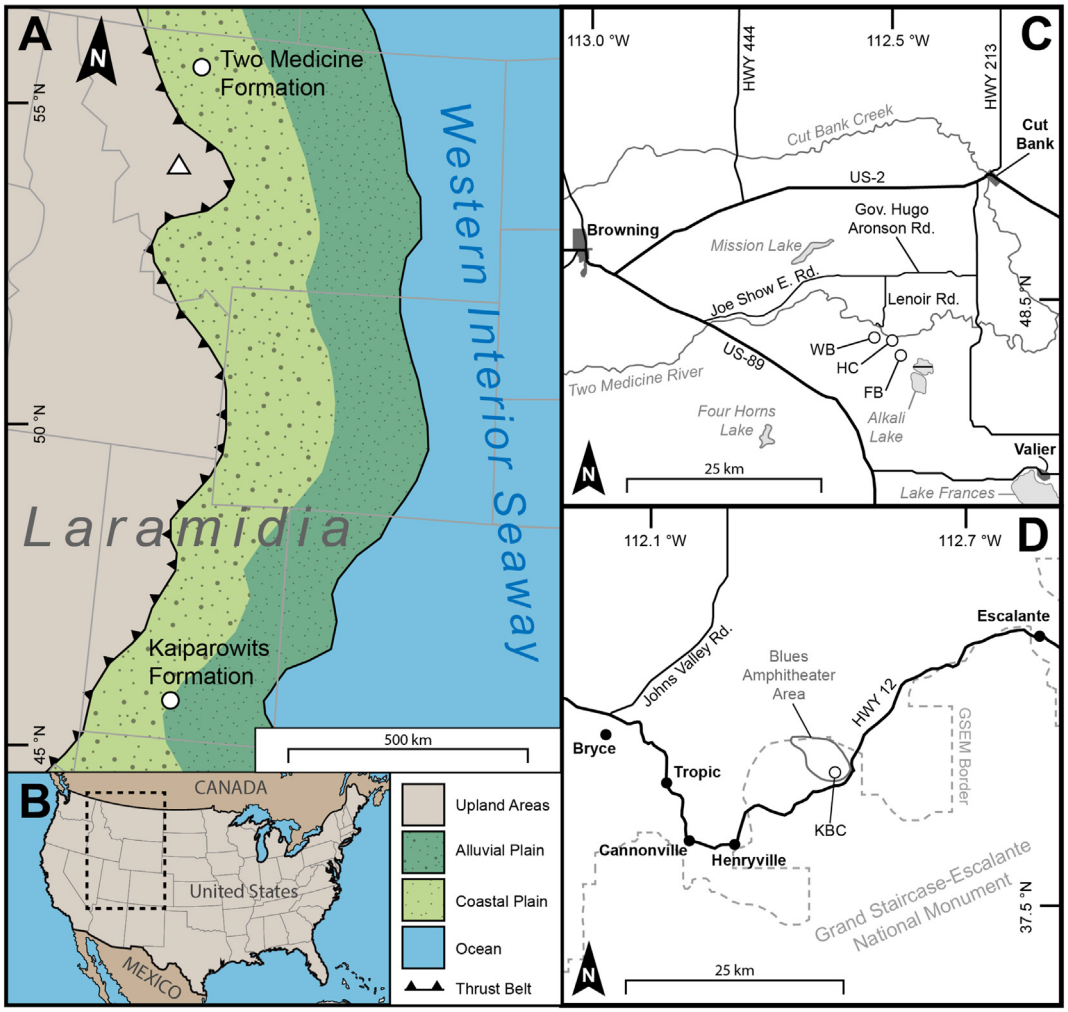

Fig. 1. A) The western margin of the Western Interior Seaway during the late Campanian (~75 Ma; paleogeography based on Gates et al., 2010 and Roberts and Kirschbaum, 1995). The Kaiparowits Formation (KBC – Kaiparowits Blues Ceratopsian) and Two Medicine Formation study areas are marked with white circles (WB – Western Butte, HC – Hagan's Crossing, FB – Flag Butte). White triangles show the position of active volcanic centers. Paleolatitudes from Miller et al. (2013). B) Locator map; dashed black line shows the location of A. C) Two Medicine Formation study area near Cut Bank and Browning, Montana. D) Kaiparowits Formation study area near Bryce and Escalante, Utah.

clumped and stable isotope variability in each paleosol. Additionally, samples of bulk soil sediment were collected from the identified soil horizons (e.g., A, Bt, Bk, etc.) for whole rock geochemistry analysis. The KF samples were collected from the formation's proposed type locality (KBC locality) as identified by Roberts (2007), while the TMF samples were collected from three sections (Hagan's Crossing, Flag Butte, and West Butte) that were previously correlated by Rogers (1995) based on the stratigraphic position of a through-going regional unconformity and a distinct, widespread interval of lacustrine deposits.

3.2. Clumped and stable isotope analyses

Carbonate clumped-isotope thermometry is a thermodynamics-based measurement of carbonate formation temperature based on the ratio of multiply substituted isotopologues in a carbonate sample (e.g., the number of carbonate molecules that contain both a heavy ^{13}C and heavy ^{18}O isotope; Ghosh et al., 2006; Eiler, 2007, 2011; Eiler et al., 2014). Using this method, the clumped isotope composition (written as Δ_{47}) of soil carbonates can be used to estimate the carbonate formation temperature ($T[\Delta_{47}]$).

Clumped and stable isotope analyses (Δ_{47}, $\delta^{18}O$, and $\delta^{13}C$) of carbonate nodules (53 samples) were conducted at the University of

Table 1
Basic information for the measured Kaiparowits and Two Medicine sections.

Formation	Section name	Section abbreviation	Latitude[a] (°N)	Longitude (°W)	Paleolatitude[b] (°N)	Number of Paleosols
Kaiparowits	Blue Ceratopsion	KBC	37.625	111.887	46.2	19
Two Medicine	Flag Butte	FB	48.441	112.489	56.5,53.4	12
Two Medicine	Hagan's Crossing	HC	48.455	112.502	56.5,53.4	15
Two Medicine	Western Butte	WB	48.461	112.527	56.5,53.4	16

[a] Coordinates mark the location of the section base.
[b] Paleolatitude from Miller et al. (2013).

Washington's IsoLab (detailed methods in Burgener et al., 2016; Kelson et al., 2017; and Schauer et al., 2016). Micritic carbonate was sub-sampled from each nodule using a Merchantek micro-mill. For some of the diagenetically altered samples, only a single replicate measurement was performed. For the remaining samples, 2 to 6 replicate analyses were performed. Carbonate samples were digested in a common phosphoric acid bath at 90 °C, and the evolved CO_2 was then cryogenically separated from water and cleaned on an automated vacuum line. Carbonate standards or equilibrated CO_2 reference gases were processed between every 4–5 sample unknowns. The purified CO_2 was analyzed on a Thermo MAT253 configured to measure m/z 44–49 inclusive.

Δ_{47}, $\delta^{13}C$, and $\delta^{18}O$ values were calculated for all samples following the methods of Huntington et al. (2009) and He et al. (2012), and were corrected for ^{17}O interference using the parameters described in Brand et al. (2010) (see Daëron et al., 2016 and Schauer et al., 2016). The carbonate Δ_{47} values were calibrated to the carbon dioxide equilibrium scale, or Absolute Reference Frame (ARF), following the methods of Dennis et al. (2011) using CO_2 gas equilibrated at 4, 60, and 1000 °C, with the exception that no acid fractionation factor was applied to correct the values to a 25 °C reference frame. We also analyzed two internal clumped isotope standards (C64 and Coral) and four inter-laboratory standards (ETH-1, ETH-2, ETH-3, and ETH-4, Bernasconi et al., 2018; Meckler et al., 2014) (see Table 2 for the associated $\delta^{18}O$, $\delta^{13}C$, and Δ_{47} values). $\delta^{13}C$ was referenced to international standards NBS-19 and LSVEC, and $\delta^{18}O$ was referenced to NBS-18 and NBS-19. The Pierce outlier test was used to identify and remove statistical outliers in the Δ_{47} values for each of the samples (Ross, 2003; Zaarur et al., 2013). Carbonate formation temperatures (T[Δ_{47}]) were calculated from the Δ_{47} results using the Δ_{47}-T calibration of Kelson et al. (2017), which was produced in the same laboratory using the same methods:

$$\Delta_{47} = \frac{0.0417 \pm 0.0013 \times 10^6}{T^2} + 0.139 \pm 0.014 \quad (1)$$

where T is temperature in Kelvin.

3.3. Diagenetic screening methods

Alteration of the primary clumped and stable isotope compositions of soil carbonate nodules via diagenesis can potentially destroy or modify any climate signals preserved in the samples. To avoid sampling altered material, the carbonate nodules collected for this study were assessed for alteration based on textural, cathodoluminescence (CL), and isotopic evidence. We assigned each thin-sectioned nodule to one of three categories (micritic, mixed, or sparry) based on the observed abundance, spacing (e.g., distributed evenly throughout the nodule or restricted to isolated veins), and luminescence of diagenetic sparry calcite (Fig. 2). Optical and CL observations of the thin sections were made using a Nikon Optiphot-2 microscope and Luminiscope ELM-3R CL system. Nodules were assigned to the micritic category if they were composed of homogenous micrite with a low luminescence. Nodules containing high luminescence spar were assigned to the mixed category if the spar was restricted to isolated veins or zones and the remaining micrite was easily sub-sampled, or to the sparry category if the nodule was composed completely of highly luminescent spar or if spar was pervasive throughout the nodule.

3.4. Mean annual temperature and precipitation calculations from whole rock geochemistry

Several past studies have attempted to reconstruct MAAT and MAP from paleosol bulk geochemistry using the PWI and CIA-K methods, respectively (e.g., Driese et al., 2016; Schatz et al., 2015; Smith et al., 2015); accordingly, we apply these methods to KF and TMF to evaluate their utility in these deposits. The major-element composition of 25 bulk paleosol sediment samples from 12 individual Bt horizons and 5 well-developed soil profiles were measured by X-ray fluorescence (XRF) at the ALS Chemex Laboratory in Reno, Nevada. The Bt horizon compositions were used to calculate estimates of the time-averaged mean annual temperature (MAT) and mean annual precipitation (MAP) for each sample. MAT was calculated using the PWI method described by Gallagher and Sheldon (2013). The PWI is a modified version of the index of weathering developed by Parker (1970) that estimates the extent of soil weathering based on the abundance of two cations that are highly susceptible to leaching during chemical weathering (Na and K) and two resistant cations (Mg and Ca). To calculate PWI, the relative molar abundance of each of these cations is divided by the cation's bond strength and percent ionic character, and the resulting values are then summed, resulting in the following equation:

$$PWI = 100 \times [(4.20 \times Na) + (1.66 \times Mg) + (5.54 \times K) + (2.05 \times Ca)] \quad (2)$$

The PWI value of a Bt horizon can then be related to MAT by the following empirically-derived expression:

$$MAT(^{\circ}C) = -2.74 \times \ln(PWI) + 21.39 \quad (3)$$

The PWI paleothermometer should not be applied to paleosol horizons with a PWI over 60, because such high PWI values indicate little to no chemical weathering has taken place (Gallagher and Sheldon, 2013).

MAP was calculated using the CIA-K proxy, which was first developed by Maynard (1992). This proxy is based on the observation that modern soils that receive higher MAP also experience higher degrees of chemical weathering (Sheldon et al., 2002). CIA-K is calculated based on the molar ratio of Al_2O_3 to Al_2O_3, CaO, and Na_2O as follows:

$$CIA - K = 100 \times \left(\frac{Al_2O_3}{Al_2O_3 + CaO + Na_2O} \right) \quad (4)$$

The Bt horizon CIA-K value can then be related to calculate MAP using the empirically-derived expression (Sheldon et al., 2002 (right?)):

$$MAP(mm\ yr^{-1}) = 221.1e^{0.0197(CIA-K)} \quad (5)$$

Table 2
Clumped isotope calcite standards, accepted and measured values.

Standard	Accepted $\delta^{13}C$ (‰) VPDB	Measured $\delta^{13}C$ (‰) VPDB	± 1 SE (‰)	Accepted $\delta^{18}O$ (‰) VPDB	Measured $\delta^{18}O$ (‰) VPDB	± 1 SE (‰)	Accepted Δ_{47} (‰)	Measured Δ_{47} (‰)	± 1 SE (‰)
C64[a]	−2.05	−2.05	0.01	−15.54	−15.66	0.02	0.5250	0.5250	0.0160
C2[b]	−48.93	−48.93	0.013	−16.49	−16.48	0.015	0.5200	0.5337	0.0326
Coral[a]	−2.14	−2.30	0.015	−4.50	−4.51	0.018	0.6220	0.6274	0.0239
ETH-1[c]	2.14	2.10	0.015	−2.18	−2.18	0.029	0.2050	0.2089	0.0361
ETH-2[c]	−10.10	−10.11	0.029	−18.76	−18.48	0.074	0.1990	0.2458	0.0550
ETH-3[c]	1.81	1.75	0.031	−1.77	−1.79	0.023	0.6120	0.6236	0.0282
ETH-4[c]	−10.11	−10.20	0.013	−18.82	−18.66	0.022	0.4530	0.4513	0.0215

[a] University of Washington Isolab in-house standard.
[b] University of Washington Isolab in-house standard, Merck Suprapur Calcim carbonate product number 1020590050.
[c] Interlaboratory clumped isotope standard.

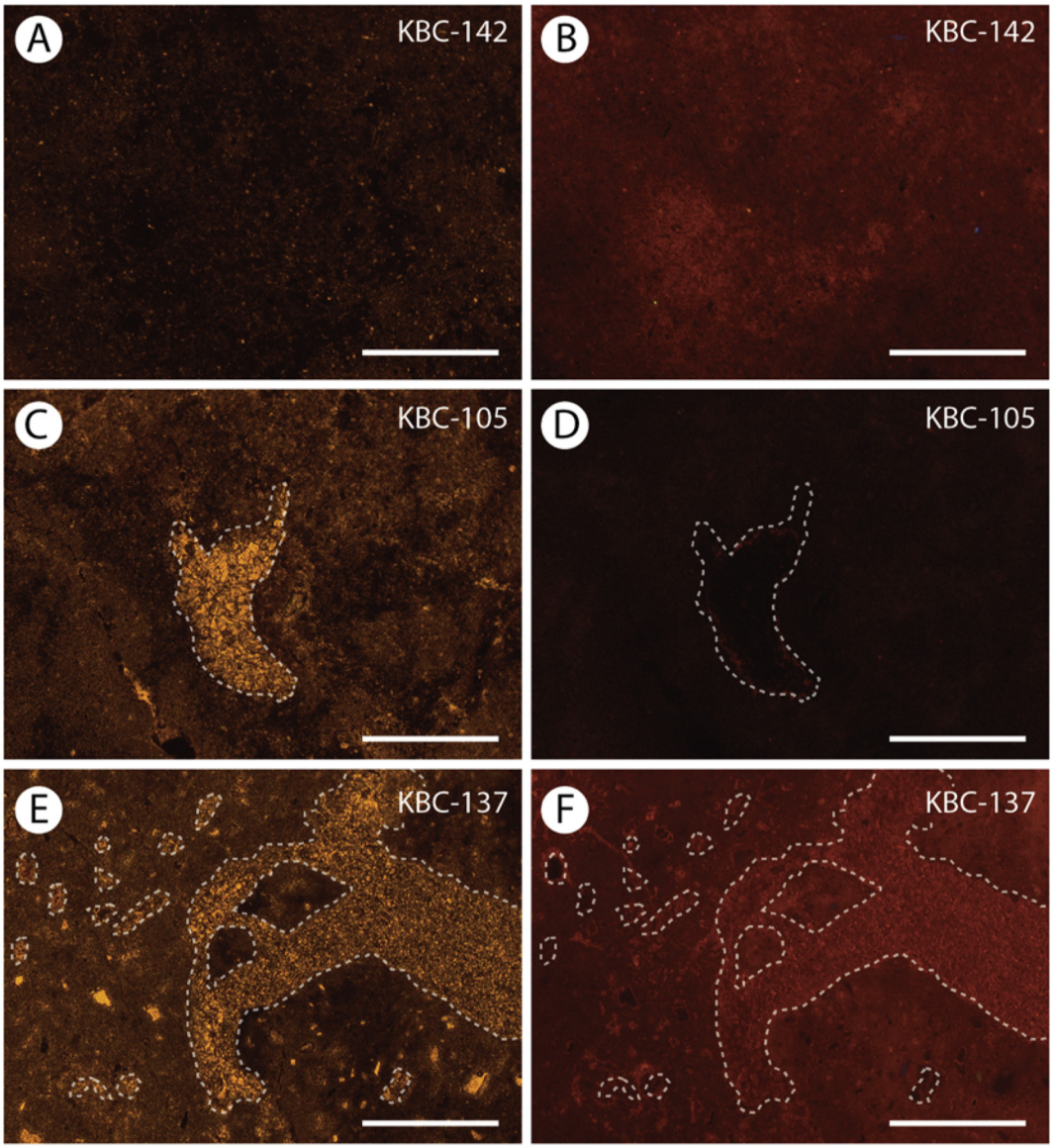

Fig. 2. Optical (left) and cathodoluminescence (right) thin section images for micritic (A, B), mixed (C, D) and sparry (E,F) samples. Scale bars are 500 μm. White dashed lines highlight spar-filled voids and fractures in the mixed and sparry samples.

3.5. Modern climate, soil, and land cover data

To provide context for our Late Cretaceous MART reconstructions, we analyzed modern climate reanalysis output and soil and temperature data from the soil climate analysis network (SCAN). To calculate modern MART, we used mean monthly 2-meter air temperature output (1981 to 2016) from the ERA-Interim climate reanalysis project (spatial resolution = 0.75 °; Dee et al., 2011; https://www.ecmwf.int/en/forecasts/datasets/reanalysis-datasets/era-interim). This modern reanalysis dataset was also compared to different land cover types using the MODIS land cover dataset developed by Channan et al. (2014) and Friedl et al. (2010), to understand how MART varies by environment. We calculated soil radiative heating (ST_{RH}) by taking the difference between SCAN station soil and air temperatures for three different summer periods: 1) mean summer temperature (June, July, August); 2) warmest-month mean temperature; and 3) warmest-month mean maximum daily temperature. We used long-term soil and air data from 199 SCAN weather stations in the continental United States and Alaska (Supplementary Table 1; SCAN is maintained and distributed as a joint project of the National Water and Climate Center and the Natural Resources Conservation Service; https://www.wcc.nrcs.usda.gov/scan/). We note that there is a significant bias to the location of the SCAN weather stations, with just seven states (Alaska, Alabama, California, Mississippi, Nevada, Texas, and Utah) containing 59% of all stations. Despite this, the stations cover a wide range of environments over a latitudinal range from 20 to 66 °N, with a gap from 48 to 59 °N.

4. Results

4.1. Paleosol mapping results

We identified 19 individual paleosols (2 truncated) from the type stratigraphic section in the KF, and 43 paleosols (13 truncated) from three correlated stratigraphic sections (Figs. 3 and 4; Supplementary Table 2) in the TMF. The KF section shows a distinct evolution in paleosol morphology with stratigraphic height. The first paleosol-bearing portion of the section (221 to 355 m) is ~130 m thick and contains just three widely spaced but well-developed paleosols that are relatively thick (> 200 cm), and contain distinct A, Bt, and Bk horizons. The middle 65 m of the section (361 to 426 m) are typified by much thinner

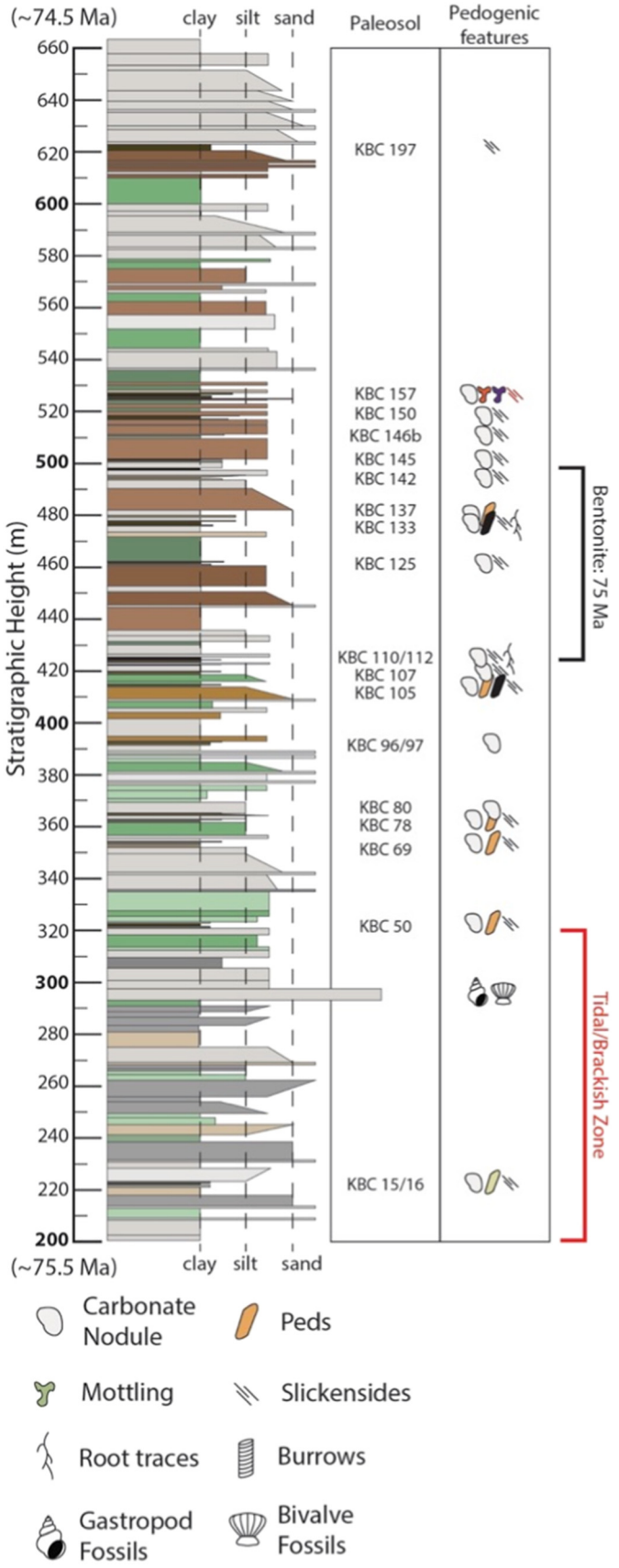

Fig. 3. Stratigraphic column for the Kaiparowits Formation Blue Ceratopsian (KBC) section. Non-paleosol stratigraphic data from Roberts, 2005. Colors correspond to Munsell soil colors for fresh bulk sediment samples (see Supplementary Table 2). (For interpretation of the references to color in this figure legend, the reader is referred to the web version of this article.)

paleosols (~120 cm) with 10 to 20 cm A horizons and Bk or Bkt horizons characterized by weak or completely absent clay accumulation. The upper paleosol-bearing portion of the section is ~68 m thick (460 to 528 m), and shows a return to well-developed paleosols with A, Bt, and Bk horizons, though these upper paleosols are generally thinner (~150 cm) than the lowermost KF paleosols. All of the KF paleosols are drab gray or gray-green in color, contain abundant but small (maximum size < 1.5 cm) carbonate nodules, rare mottling and root traces, and rare ped development (though ped surfaces are commonly oxidized). Based on these observations, we organize the KF paleosols into two taxonomic groups: the Powell Point (Calcic Argillisol/Calcic Alfisol) and Blues Amphitheater (Calcic Protosol/Calcic Inceptisol) pedotypes (Fig. 5A and B; e.g., Retallack, 1994). Qualitative estimates of the minimum duration of pedogenic activity for the KF paleosols based on the average size of the carbonate nodules yield values of 3 to 4 ka for the KF paleosols (e.g., Retallack, 2005).

The TMF section is distinguished by abundant truncated paleosols (30% of the identified TMF paleosols), and by a higher proportion of non-calcic paleosols compared to the KF section (~40% of TMF paleosols versus ~10% of the KF paleosols). The first 25 m of the Western Butte section are characterized by three well-developed carbonate bearing paleosols with distinct A, Bt, and Bk/Bkt horizons interspersed with five truncated Bk/Bkt horizons and a single thin argillic paleosol. The section abruptly transitions from this carbonate nodule-rich section to a 17 m sequence of predominantly purple argillic paleosols with complete A and Bt horizons. The lower 30 m of the Hagan's Crossing section contain alternating carbonate-bearing and clay-rich paleosols topped by two truncated Bkt horizons. The upper portion of the Hagan's Crossing section contains predominantly carbonate-bearing paleosols, as well as two relatively thick Histosols. The first four paleosols in the Flag Butte section are truncated Bk or Bkt horizons, while the remainder of the section is characterized by relatively well-developed paleosols with distinct A, Bt, and Bk horizons, usually argillic paleosols with either Bt or Bk horizons. At all three TMF sections, the Bk and Bkt horizons are particularly well developed and yield abundant carbonate nodules that are typically much larger than those found in the KF paleosols (up to 2.4 cm). Slickensides and organic plant matter are relatively rare in the TMF paleosols, while mottling, ped development, and root traces are more common than in the KF paleosols. We classify the TMF paleosols into three taxonomic groups: the Western Butte (Argillisol/Alfisol), Hagan's Crossing (Calcisol/Aridisol), and Flag Butte (Calcic Argillisol/Calcic Alfisol) pedotypes (Fig. 5C, D, and E). The minimum duration of pedogenic activity for the TMF paleosols based on the average size of the carbonate nodules ranges from 2 to 5 ka.

4.2. Clumped and stable isotope results

Based on the diagenetic assessment described in Section 3.5 of this study, we assigned the KF and TMF carbonate nodules to one of three categories: micritic, mixed, or sparry (Table 3). The micritic KF ($n = 4$) and TMF ($n = 12$) paleosol carbonate $\delta^{18}O$ (VPDB) values range from −7.7 to −7.5‰ (± 0.1‰) and from −11.9 to −9.0‰ (± 0.1‰), respectively (Table 3, Supplementary Tables 3 and 4). Their $\delta^{13}C$ (VPDB) values range from −9.6 to −8.5‰ (± 0.1‰) and from −8.6 to −6.7‰ (± 0.1‰), respectively. These values are indistinguishable from $\delta^{18}O$ and $\delta^{13}C$ values reported for KF and TMF paleosol carbonates by Foreman et al. (2011, 2015) and Snell et al. (2014). The mean $T(\Delta_{47})$ value for the micritic KF is 35 ± 4 °C, and 33 ± 4 °C for the micritic TMF. With only four pristine carbonate samples, the KF record is too sparse to determine if there is a temporal trend in the data, and the TMF $T(\Delta_{47})$ values for the micritic nodules (n = 12) show little variation with stratigraphic height (Supplementary Figs. 1 and 2). We note that the TMF $T(\Delta_{47})$ values are consistent with the single paleosol carbonate and two lacustrine carbonate clumped isotope temperatures reported by Snell et al. (2014) (mean $T(\Delta_{47}) = 31$ °C). The KF and TMF carbonates classified as mixed or sparry samples yield $\delta^{18}O$ (VPDB) values

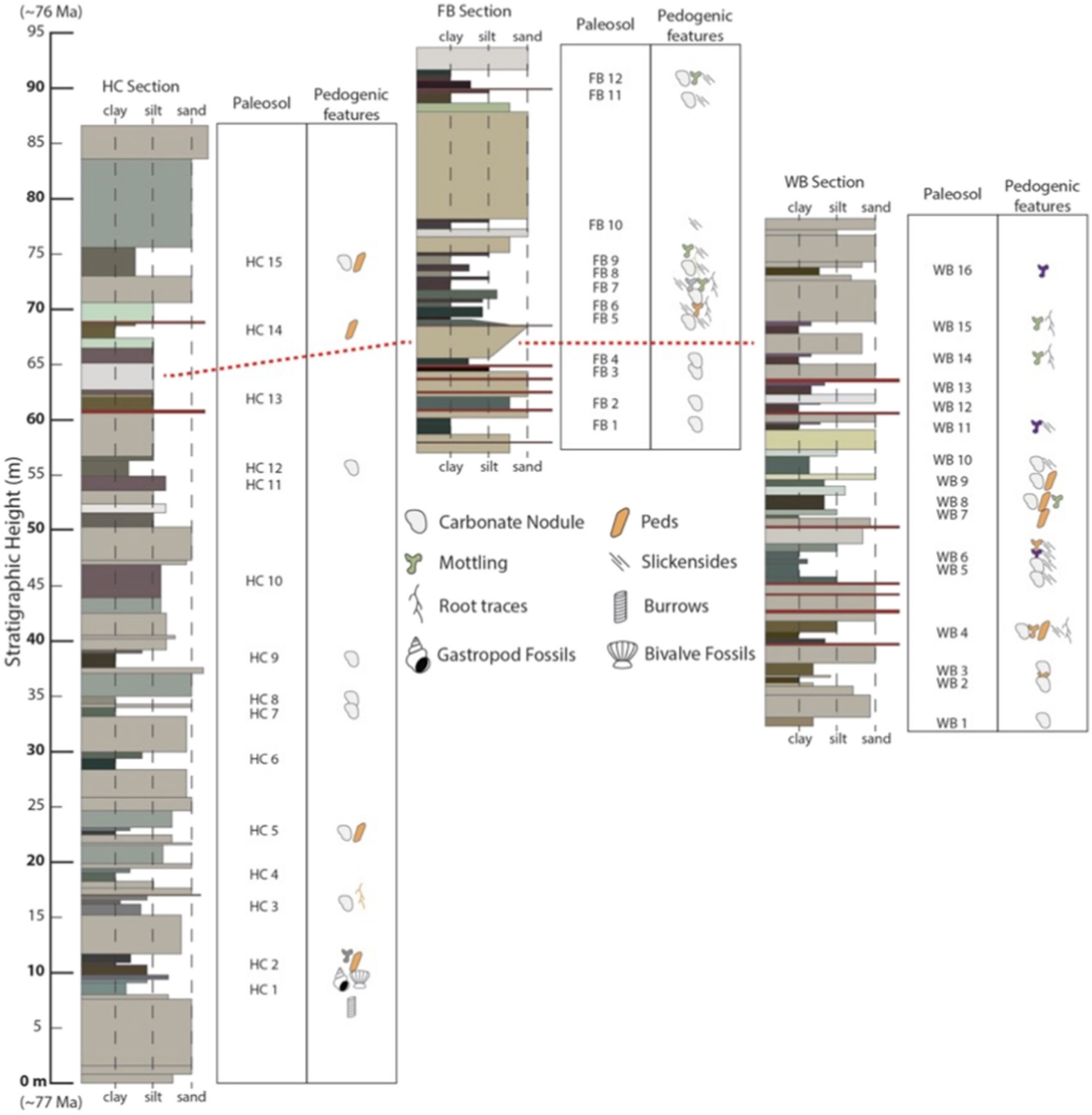

Fig. 4. Stratigraphic column for the Two Medicine Formation Hagan's Crossing (HC), Flag Butte (FB), and Western Butte (WB) sections. Colors correspond to Munsell soil colors for fresh bulk sediment samples (see Supplementary Table 2).

that range from −9.1 to −7.3‰ (± 0.1‰) and − 11.4 to −9.8‰ (± 0.2‰), respectively, while the $\delta^{13}C$ (VPDB) values range from −9.4 to −7.4‰ (± 0.1‰) and − 9.1 to −7.1‰ (± 0.1‰), respectively. The mixed samples yield a mean $T(\Delta_{47})$ value of 43 ± 6 °C and 40 ± 5 °C for the KF and TMF samples, respectively. The mean $T(\Delta_{47})$ value of the KF sparry samples is 41 ± 5 °C, and 42 ± 6 °C for the TMF sparry samples (Supplementary Fig. 3).

The spar from one KF and three TMF carbonate nodules (KBC-137s, TM-HC-1s, TM-HC-7s, TM-WB-6s) was subsampled to characterize its isotopic composition. The $\delta^{18}O$, $\delta^{13}C$, and $T(\Delta_{47})$ values of the KF spar sample was not distinguishable from those of the other KF samples. Due to the small size of the KF nodules and the observed heterogeneous mixture of micritic and sparry calcite in the KBC-137s nodule, we suspect that some micritic material was accidentally incorporated into this "spar" sample. In contrast, the TMF spar samples yield high $T(\Delta_{47})$ values (μ = 62 ± 10 °C) and show a clear pattern of decreasing $\delta^{18}O$ values and increasing $\delta^{13}C$ values relative to the micritic, mixed, and sparry TMF carbonates (Fig. 6). The variability in the $\delta^{18}O$ and $\delta^{13}C$ of the sparry, mixed, and micritic carbonates, as well as the variability in luminescence observed during the CL analysis (Fig. 2B, D, and F) may suggest that multiple, chemically distinct fluids caused the alteration observed in the sparry and mixed carbonates.

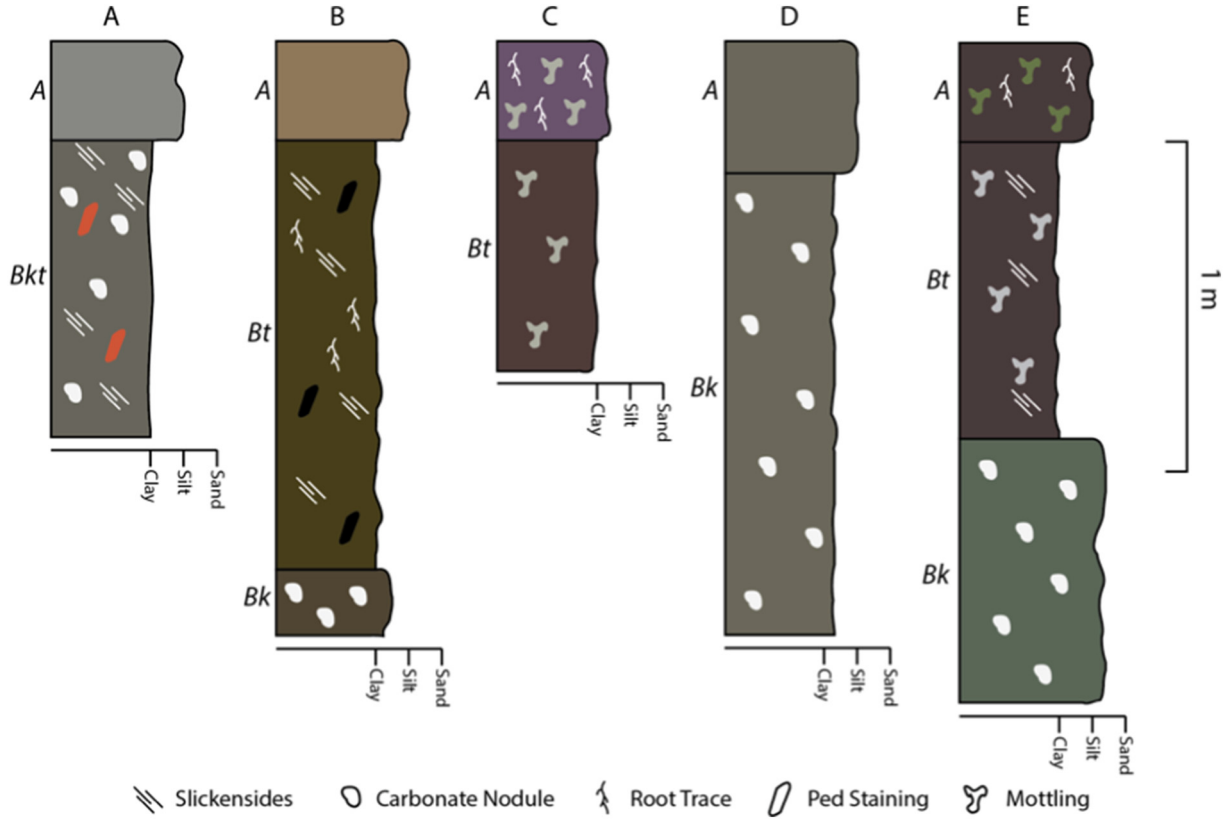

Fig. 5. Type paleosol profiles for the Blues Amphitheater Protosol/Inceptisol (A), Powell Point Argillisol/Alfisol (B), Western Butte Argillisol/Alfisol (C), Hagan's Crossing Calcisol/Aridisol (D), and Flag Butte Argillisol/Alfisol (E) pedotypes. Thicknesses displayed are averages for each pedotype.

4.3. Late Cretaceous MAAT and MAP from paleosol bulk geochemistry

The paleosol bulk geochemistry analyses for the KF and TMF paleosols yield Ti/Al ratios that are constant with stratigraphic height (KF: $\mu = 0.05$, $\sigma = 0.004$; TMF: $\mu = 0.03$, $\sigma = 0.009$), indicating that both locations experienced little or no provenance change over the measured interval (Hyland et al., 2017; Sheldon and Tabor, 2009). MAAT was calculated only for those Bt horizons that had PWI values that were both < 60 and lower than the PWI of the underlying parent material (Gallagher and Sheldon, 2013). The KF and TMF both yield a mean PWI MAAT value of 11 ± 2 °C (Table 4). For the CIA-K proxy, mean MAP values for the KF and TMF are 960 ± 190 and 860 ± 200 mm yr^{-1}, respectively (Table 4). Sample TM-HC-2-Bt yielded CIA-K values that were too similar to the underlying parent material (CIA-K difference < 8), indicating that the soil had not experienced enough weathering to apply the CIA-K proxy. This sample was not included in the MAP calculations.

5. Discussion

In the following sections, we present our interpretations of the paleosol carbonate and bulk geochemistry data and our subsequent estimates of Late Cretaceous MART. The $T(\Delta_{47})$ values of our pristine (micritic) and altered (mixed and sparry) paleosol carbonate nodules are reviewed, and the SCAN data results are used to constrain the amount of radiative heating the KF and TMF paleosols likely experienced during soil carbonate formation. The accuracy of our new MAT and MAP reconstructions based on the PWI and CIA-K proxies are discussed in the context of paleosol characteristics and previous quantitative and qualitative proxy estimates. Possible causes for the unexpectedly low PWI and CIA-K values are discussed, and previous proxy MAT and MAP values are selected to use in the MART calculations. We discuss the uncertainties associated with our Late Cretaceous MART and cold-month mean temperature estimates in light of modern MART estimates based on ERA-Interim climate reanalysis data. We compare our Late Cretaceous MART estimates to previous leaf physiognomy MART estimates and to model simulations for the same period. Finally, we compare these Late Cretaceous MART estimates to modern MART and discuss the implications of our findings for understanding greenhouse climates.

5.1. Interpreting Late Cretaceous summer air temperatures from paleosol carbonate $T(\Delta_{47})$ values

The mixed and sparry KF and TMF samples show textural and clumped isotopic evidence of being compromised to some degree by diagenetic alteration. In both the mixed and sparry samples, our petrographic analysis shows that void spaces and fractures have been filled to varying extents by coarse-grained, sparry calcite indicative of post-burial diagenesis. Supplementary Fig. 3 shows that the mixed and sparry samples have more negative $\delta^{18}O$ values relative to the micritic samples, and more variability in $T(\Delta_{47})$ values. Additionally, the mixed and sparry KF and TMF samples yield high mean $T(\Delta_{47})$ values of 42.1 ± 5.3 and 41.3 ± 5.8 °C, respectively, which are 7 to 9 °C hotter than the mean $T(\Delta_{47})$ values of the micritic carbonates (Supplementary Fig. 3E and 3F).

Based on the evidence presented above, we chose to treat all of the mixed and sparry KF and TMF samples as being compromised by some degree of diagenesis, and did not include those samples in our calculations of MART. In contrast, the remaining samples 1) have a fine-grained, micritic texture consistent with unaltered pedogenic carbonate, and 2) yield consistent, reasonable Earth-surface $T(\Delta_{47})$ values (< 40 °C), which leads us to classify them as unaltered, pristine carbonate.

We interpret the mean KF and TMF $T(\Delta_{47})$ values of the micritic carbonates (35 ± 4 °C and 33 ± 4 °C, respectively) as being consistent

Table 3
Clumped and stable isotope results.

Sample name	Formation	Section	Stratigraphic height	n	Fabric classification	$\delta^{13}C_{carb}$ (‰) VPDB	± 1 SE (‰)	$\delta^{18}O_{carb}$ (‰) VPDB	± 1 SE (‰)	$\delta^{18}O_{water}$ (‰) VSMOW	± 1 SE (‰)	Δ_{47}	± 1 SE (‰)	$T(\Delta_{47})$	± 1 SE (‰)
TM-HC-1	Two Medicine	Hagan's Crossing (HC)	8.2	2	Sparry	−7.84	0.08	−9.83	0.03	−2.49	0.03	0.563	0.012	40	4
TM-HC-1b	Two Medicine	Hagan's Crossing (HC)	8.2	3	Mixed	−8.24	0.07	−9.99	0.47	−3.91	0.47	0.578	0.009	35	3
TM-HC-1s	Two Medicine	Hagan's Crossing (HC)	8.2	2	Spar	−6.39	0.13	−12.32	0.08	−0.21	0.08	0.556	0.052	45	20
TM-HC-3	Two Medicine	Hagan's Crossing (HC)	16.4	2	Mixed	−7.12	0.00	−9.88	0.00	−0.93	0.00	0.551	0.016	45	6
TM-HC-3b	Two Medicine	Hagan's Crossing (HC)	16.4	2	Sparry	−8.17	0.02	−9.92	0.06	−3.06	0.06	0.570	0.044	39	16
TM-HC-3c	Two Medicine	Hagan's Crossing (HC)	16.4	3	Micritic	−6.65	0.05	−9.53	0.46	−2.99	0.46	0.588	0.009	31	3
TM-WB-1a	Two Medicine	Western Butte (WB)	33	4	Micritic	−7.87	0.08	−10.04	0.07	−2.95	0.07	0.571	0.016	38	6
TM-WB-1b	Two Medicine	Western Butte (WB)	33	3	Micritic	−7.95	0.01	−10.03	0.06	−3.43	0.06	0.576	0.018	36	7
TM-HC-7	Two Medicine	Hagan's Crossing (HC)	33.2	3	Micritic	−8.06	0.01	−9.45	0.05	−3.72	0.05	0.578	0.009	35	3
TM-HC-7s	Two Medicine	Hagan's Crossing (HC)	33.2	2	Spar	−4.58	0.10	−15.77	0.12	7.90	0.12	0.465	0.012	85	6
TM-HC-9	Two Medicine	Hagan's Crossing (HC)	37.6	3	Sparry	−9.09	0.00	−10.08	0.09	−3.63	0.09	0.561	0.009	41	3
TM-WB-3	Two Medicine	Western Butte (WB)	37.6	3	Micritic	−7.66	0.01	−8.97	0.08	−4.67	0.08	0.599	0.009	28	3
TM-WB-5	Two Medicine	Western Butte (WB)	46	1	Sparry	−7.92	0.06	−11.42	0.13	−0.68	0.13	0.535	0.016	51	6
TM-WB-6	Two Medicine	Western Butte (WB)	47.7	4	Mixed	−8.59	0.05	−9.91	0.15	−2.30	0.15	0.549	0.008	46	3
TM-WB-6s	Two Medicine	Western Butte (WB)	47.7	2	Spar	−7.19	0.07	−13.21	0.14	0.86	0.14	0.524	0.012	56	5
TM-WB-8	Two Medicine	Western Butte (WB)	52.1	4	Micritic	−7.83	0.07	−9.89	0.10	−4.30	0.10	0.590	0.009	31	3
TM-FB-1	Two Medicine	Flag Butte (FB)	59.7	4	Micritic	−7.44	0.04	−9.55	0.02	−3.60	0.02	0.586	0.008	32	3
TM-HC-13	Two Medicine	Hagan's Crossing (HC)	60.9	2	Sparry	−7.96	0.02	−10.43	0.06	−1.67	0.06	0.549	0.014	46	5
TM-HC-13b	Two Medicine	Hagan's Crossing (HC)	60.9	2	Sparry	−8.22	0.27	−9.77	0.14	−1.61	0.14	0.545	0.018	48	7
TM-FB-3	Two Medicine	Flag Butte (FB)	64.4	3	Micritic	−7.21	0.02	−9.97	0.05	−3.13	0.05	0.582	0.014	34	5
TM-FB-5	Two Medicine	Flag Butte (FB)	68.6	2	Mixed	−8.56	0.09	−11.12	0.01	−4.25	0.01	0.579	0.024	35	8
TM-FB-5b	Two Medicine	Flag Butte (FB)	68.6	2	Sparry	−8.13	0.11	−11.33	0.03	−2.46	0.03	0.558	0.012	42	4
TM-FB-5c	Two Medicine	Flag Butte (FB)	68.6	2	Micritic	−8.46	0.25	−11.34	0.16	−3.92	0.16	0.575	0.012	36	4
TM-FB-7	Two Medicine	Flag Butte (FB)	70.9	2	Micritic	−8.53	0.13	−11.86	0.26	−5.69	0.26	0.601	0.012	27	4
TM-FB-7b	Two Medicine	Flag Butte (FB)	70.9	4	Micritic	−8.59	0.02	−11.89	0.24	−3.85	0.24	0.572	0.009	37	3
TM-HC-15	Two Medicine	Hagan's Crossing (HC)	73.1	3	Sparry	−7.48	0.03	−11.41	0.06	−3.70	0.06	0.587	0.009	32	3
TM-FB-11b	Two Medicine	Flag Butte (FB)	88.6	5	Micritic	−7.59	0.02	−11.10	0.03	−5.34	0.03	0.611	0.011	24	4
KBC-15	Kaiparowits	Blue Ceratopsian (KBC)	222.8	2	Bulk	−6.40	0.12	−10.04	0.03	−0.23	0.03	0.551	0.012	45	4
KBC-15b	Kaiparowits	Blue Ceratopsian (KBC)	222.8	1	Mixed	−7.43	0.06	−9.04	0.13	−0.10	0.13	0.534	0.016	52	6
KBC-50	Kaiparowits	Blue Ceratopsian (KBC)	321.6	2	Bulk	−9.87	0.00	−7.99	0.02	−3.85	0.02	0.553	0.012	44	4
KBC-69	Kaiparowits	Blue Ceratopsian (KBC)	353.5	2	Bulk	−9.01	0.04	−8.59	0.01	−4.17	0.01	0.571	0.012	38	4
KBC-69b	Kaiparowits	Blue Ceratopsian (KBC)	353.5	2	Mixed	−9.36	0.13	−7.61	0.18	−2.39	0.18	0.540	0.020	50	8
KBC-69c	Kaiparowits	Blue Ceratopsian (KBC)	353.5	2	Micritic	−9.33	0.06	−7.64	0.06	−4.95	0.06	0.577	0.012	35	4
KBC-80	Kaiparowits	Blue Ceratopsian (KBC)	365	2	Bulk	−8.25	0.46	−8.31	0.14	0.51	0.14	0.514	0.012	60	5

(*continued on next page*)

Table 3 (*continued*)

Sample name	Formation	Section	Stratigraphic height	n	Fabric classification	$\delta^{13}C_{carb}$ (‰) VPDB	± 1 SE (‰)	$\delta^{18}O_{carb}$ (‰) VPDB	± 1 SE (‰)	$\delta^{18}O_{water}$ (‰) VSMOW	± 1 SE (‰)	Δ_{47}	± 1 SE (‰)	T(Δ_{47})	± 1 SE (‰)
KBC-80b	Kaiparowits	Blue Ceratopsian (KBC)	365	2	Bulk	−8.37	0.04	−7.87	0.03	−2.75	0.03	0.559	0.012	42	4
KBC-96	Kaiparowits	Blue Ceratopsian (KBC)	392.6	4	Bulk	−8.96	0.01	−8.31	0.02	−3.57	0.02	0.563	0.014	41	6
KBC-105	Kaiparowits	Blue Ceratopsian (KBC)	414.4	3	Bulk	−9.67	0.04	−8.21	0.21	−5.51	0.21	0.581	0.009	34	3
KBC-105b	Kaiparowits	Blue Ceratopsian (KBC)	414.4	5	Micritic	−9.56	0.02	−7.74	0.04	−5.91	0.04	0.589	0.011	31	4
KBC-107	Kaiparowits	Blue Ceratopsian (KBC)	419.7	6	Bulk	−9.21	0.01	−9.13	0.13	−5.02	0.13	0.581	0.009	34	3
KBC-112	Kaiparowits	Blue Ceratopsian (KBC)	424.3	2	Sparry	−7.85	0.01	−9.06	0.09	−0.72	0.09	0.537	0.012	51	5
KBC-112b	Kaiparowits	Blue Ceratopsian (KBC)	424.3	3	Sparry	−8.28	0.01	−8.80	0.12	−2.64	0.12	0.559	0.010	42	4
KBC-125	Kaiparowits	Blue Ceratopsian (KBC)	461.3	4	Bulk	−9.02	0.06	−7.88	0.13	−4.27	0.13	0.574	0.020	37	8
KBC-125b	Kaiparowits	Blue Ceratopsian (KBC)	461.3	3	Sparry	−8.93	0.09	−7.27	0.04	−4.13	0.04	0.572	0.015	38	6
KBC-137	Kaiparowits	Blue Ceratopsian (KBC)	479.9	3	Sparry	−8.85	0.03	−8.38	0.03	−3.91	0.03	0.570	0.014	38	5
KBC-137b	Kaiparowits	Blue Ceratopsian (KBC)	479.9	3	Bulk	−9.05	0.12	−7.78	0.20	−4.06	0.20	0.569	0.015	39	6
KBC-137s	Kaiparowits	Blue Ceratopsian (KBC)	480.4	1	Spar	−8.56	0.06	−7.91	0.13	−4.58	0.13	0.583	0.016	33	6
KBC-142	Kaiparowits	Blue Ceratopsian (KBC)	494	2	Micritic	−8.48	0.00	−7.55	0.03	−4.16	0.03	0.578	0.012	35	4
KBC-142b	Kaiparowits	Blue Ceratopsian (KBC)	494	4	Micritic	−8.50	0.14	−7.48	0.22	−3.90	0.22	0.574	0.009	36	3
KBC-145	Kaiparowits	Blue Ceratopsian (KBC)	501	3	Bulk	−10.53	0.01	−7.40	0.06	−8.20	0.06	0.609	0.009	25	3
KBC-146	Kaiparowits	Blue Ceratopsian (KBC)	510.5	2	Bulk	−9.13	0.02	−9.58	0.08	−2.61	0.08	0.546	0.019	47	7
KBC-150	Kaiparowits	Blue Ceratopsian (KBC)	517.2	3	Sparry	−7.84	0.05	−8.29	0.08	−3.37	0.08	0.577	0.016	36	6
KBC-150b	Kaiparowits	Blue Ceratopsian (KBC)	517.2	3	Mixed	−9.08	0.04	−8.20	0.09	−6.00	0.09	0.597	0.010	29	3
KBC-157	Kaiparowits	Blue Ceratopsian (KBC)	525.9	5	Bulk	−9.66	0.01	−8.15	0.06	−5.85	0.06	0.587	0.012	32	4

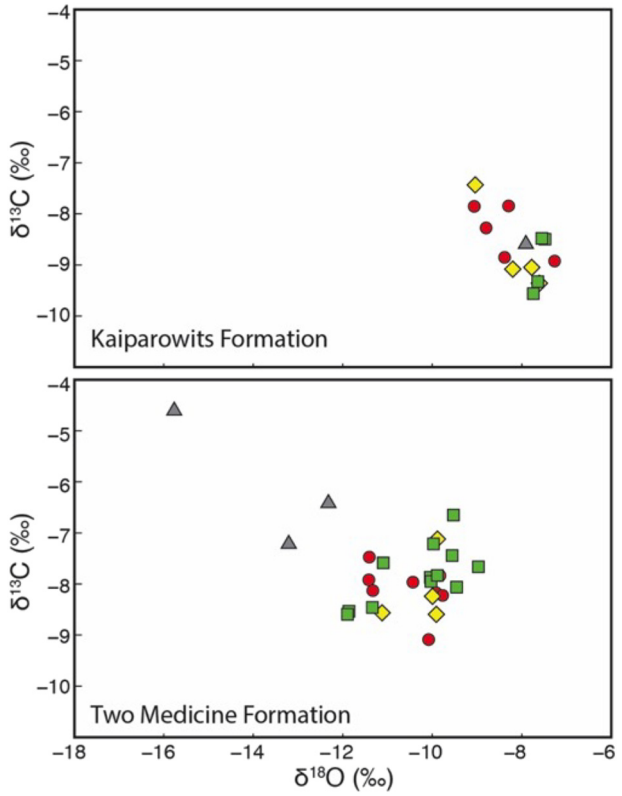

Fig. 6. Paleosol nodule carbonate $\delta^{18}O$ versus $\delta^{13}C$ (VPDB), colored by fabric classification: micritic samples (green squares), mixed samples (yellow diamonds), sparry samples (red circles), and samples of exclusively void-filling spar (gray triangles). (For interpretation of the references to color in this figure legend, the reader is referred to the web version of this article.)

with soil carbonate formation during the warmest month of the year (e.g., equivalent to warmest month mean soil temperature) for two reasons. First, multiple model simulations (Poulsen et al., 2007; Fricke et al., 2010; Kump and Slingerland, 1999; Poulsen et al., 1999) have suggested that the western margin of the WIS experienced a pronounced monsoon-like climate in both the middle and Late Cretaceous, with most precipitation falling during the warm season. The bulk oxygen isotope compositions of various carbonate materials (e.g., paleosol nodules, fossil bivalves, etc.) have been interpreted as consistent with this monsoon hypothesis (Dennis et al., 2013; Foreman et al., 2011; Fricke et al., 2010). In the modern, soil carbonate formation in hot monsoon climates is believed to occur in the warmest month just before the wet season begins (Breecker et al., 2009; Quade et al., 2013). We suggest that like modern soil carbonates in India or the southwestern United States, our Upper Cretaceous paleosol nodules formed during the warmest month of the year just prior to the beginning of monsoonal precipitation, when soils were likely at their driest. Second, studies of modern plants show that at temperatures > 35 °C, plants begin to die due to photorespiration dominating over photosynthesis (Huber, 2008; Matthews et al., 2007; Sharkey, 2000; Berry and Bjorkman, 1980), suggesting that in regions with well-established floral records such as the KF and TMF (Miller et al., 2013; Falcon-Lang, 2003), summer temperatures were likely < 40 °C. Thus maximum surface temperatures at the KF and TMF could not have been much higher than the observed $T(\Delta_{47})$ values from our paleosol carbonate samples. Our interpretation agrees with the interpretation presented in Snell et al. (2014), which is that carbonate clumped isotope temperatures from the TMF and from the Upper Cretaceous North Horn and Sheep Pass Formation (Member B) yielded a summer season bias.

Modern studies (Ringham et al., 2016; Hough et al., 2014; Quade et al., 2013; Passey et al., 2010) have suggested that the soil temperatures recorded by pedogenic carbonate clumped isotopes can be significantly higher than overlying air temperatures due to the effects of radiative soil heating. This has implications both for our interpretation of the KF and TMF $T(\Delta_{47})$ values as well as for our calculations of MART. Past studies have either converted soil carbonate $T(\Delta_{47})$ values to air temperatures by subtracting an assumed ST_{RH} value up to 6 °C in order to account for radiant ground heating (e.g., Quade et al., 2013, 2007; Snell et al., 2013), or assumed that soil carbonate $T(\Delta_{47})$ values are equivalent to air temperatures in certain locations because ST_{RH} is minimized due to vegetation shading (e.g., Hyland et al., 2018; Ghosh et al., 2016; Suarez et al., 2011).

Our review of the SCAN soil and air temperature data show that in all but the most arid environments, ST_{RH} is generally much smaller than has been assumed by previous studies like Quade et al. (2013) and Snell et al. (2013), regardless of whether it is calculated using mean summer, warmest month, or warmest-month maximum air and soil temperatures, particularly at depths relevant to carbonate proxy reconstructions (Supplementary Table 1). Mean ST_{RH} decreases with soil depth, and the maximum ST_{RH} observed for any station is 10 °C at 5 cm depth. At 50 cm depth—commonly cited as the minimum depth at which soil carbonate samples should be collected for paleoclimate analysis (Burgener et al., 2016; Quade et al., 2013; Breecker et al., 2009)— 96% of the SCAN stations have a mean warmest month ST_{RH} of < 3 °C. Importantly, the SCAN data show that only soils from arid to sub-arid environments (MAP < 600 mm yr^{-1}), where vegetation shading is limited, routinely experience warmest-month mean ST_{RH} values ≥ 5 °C, and this is typically limited to depths < 50 cm (Fig. 7). Previously reconstructed MAP values for the KF and TM ranging from ~900 to ~1780 mm yr^{-1} are significantly higher than this threshold (Miller et al., 2013; Falcon-Lang, 2003; Buck and Mack, 1995; Retallack, 1994), and the SCAN data show that for soils experiencing a similar range of MAP (900 to 1500 mm yr^{-1}), ST_{RH} at 50 cm is negligible or actually negative (i.e., warmest summer month soil temperatures are slightly cooler than air temperatures; Fig. 7). We note that radiant heating cannot cause negative ST_{RH} values; rather, the negative ST_{RH} values we report are the result of soil processes such as soil moisture effects, or the time lag in the response of a soil at depth to surface temperature changes, which lead to cooler soil temperatures relative to air temperatures (Supplementary Fig. 4). We suggest the higher ST_{RH} values observed in previous clumped isotope studies of modern soil carbonates (e.g., Burgener et al., 2016; Hough et al., 2014; Peters et al., 2013; Quade et al., 2013) were likely due to a significant sampling bias towards arid and semi-arid sites where soil carbonates are abundant and easily collected. However, these arid sites should not be taken as representative of the ST_{RH} in most soils.

Although some past clumped isotope-based studies of soil carbonates have assumed larger degrees of ST_{RH}, the relatively small degree of excess soil heating reported here is consistent with previous direct measurements of ST_{RH} (Supplementary Table 5). Passey et al. (2010) report ST_{RH} values of < 3 °C from Narok, Kenya, and negative ST_{RH} values (−1.4 to −0.4 °C) for several sites in Ethiopia and California (soil depths not reported). Cermak et al. (2016) reported a maximum ST_{RH} of 3 °C at 2 cm soil depth for three different land cover types (bare clay, bare sand, and short grass). Finally, Bartlett et al. (2006) reported long-term ST_{RH} values of < 4 °C at 2.5 cm soil depth, and negative ST_{RH} values for vegetated soils at depths > 10 cm.

Based on these findings regarding modern ST_{RH}, we calculate MART using both ST_{RH} = 0 °C and the maximum warmest month ST_{RH} correction (3 °C at 50 cm) observed for modern soils in environments with MAP values similar to the KF and TMF. Based on these two different assumptions regarding ST_{RH}, we suggest that the long-term warmest mean monthly air temperatures for the KF and TMF were 32 to 35 ± 4 °C and 30 to 33 ± 4 °C, respectively. These KF and TMF $T(\Delta_{47})$ values show that summers along the western margin of the WIS—even at paleolatitudes as high as 53 to 56 °N—were extremely hot, consistent with the global greenhouse conditions that existed at the time

Table 4
Kaiparowits and Two Medicine Formation bulk geochemistry results and paleoclimate reconstructions.

Sample name	Horizon type	Stratigraphic height (m)	Soil depth (cm)	Al_2O_3 (wt %)	CaO (wt %)	Na_2O (wt %)	MgO (wt %)	K_2O (wt %)	Ti (wt%)	CIA-K	MAP (mm yr^{-1})	PWI	MAAT (°C)					
Kaiparowits Formation																		
KBC-15-Bk	Bk	223	130	3.69	39.90	0.35	1.19	0.75	0.18	4.8		157.5		Bt	44.6	65.1		
KBC-15-Bt	Bt	223	70	13.06	2.89	1.06	3.34	2.23	0.57	65.1	797	44.6	11	Bt	40.9	69.9		
KBC-50-Bt	Bt	322	60	15.10	2.11	1.62	2.50	2.02	0.61	69.9	876	40.9	11	Bt	53.7	62.1	40.9	6.7
KBC-69-Bk	Bk	354	30	12.52	9.76	1.22	3.64	1.98	0.58	38.8		70.6		Bt	40.5	79.6		
KBC-96-Bk	Bk	393	90	14.01	0.68	1.90	2.06	2.21	0.66	76.3		36.8		Bt	37.6	84.2	73.8	8.7
KBC-107-Bk	Bk	420	75	14.61	2.08	1.95	3.07	2.31	0.61	67.6		47.0		Bt	36.2	72.8		
KBC-125-Bt	Bt	461	65	14.79	3.10	2.07	3.28	2.53	0.67	62.1	751	53.7	10	Bt	33.1	83.1		
KBC-133-Bk	Bk	476	95	9.81	18.90	1.23	2.77	1.85	0.50	21.2		99.7						
KBC-133-Bt	Bt	476.3	170	16.13	0.72	1.72	2.58	2.66	0.75	79.6	1060	40.5	11					
KBC-146B-Bt	Bt	511	60	15.77	0.32	1.45	2.01	3.11	0.73	84.2	1161	37.6	11					
KBC-150-Bt	Bt	517	75	13.80	1.41	1.58	1.73	2.25	0.72	72.8	927	36.2	12					
KBC-157-Bt	Bt	526	truncated	14.94	0.49	1.30	1.77	2.59	0.64	83.1	1137	33.1	12					
										Mean MAP (mm yr^{-1})[a]	*960 ± 190*	*MAAT (°C)[a]*	*11 ± 2*					
Two Medicine Formation																		
TM-HC-2-C	C	10	100	18.89	1.67	3.28	4.25	0.48	0.32	69.1		48.7		Bt	37.8	73.5		
TM-HC-2-Bt	Bt	11	90	15.13	0.89	2.34	3.44	0.78	0.29	73.5		37.8	11	Bt	40.9	74.4	48.3	19.4
TM-HC-2-A	A	11	40	17.03	2.06	2.46	4.56	0.95	0.34	68.6		48.6		Bt	41.4	74.5		
TM-WB-4-Bkt	Bkt	41	180	11.83	8.97	1.53	2.92	2.48	0.47	38.6		69.7		Bt	82.8	41.8	68.4	15.0
TM-WB-4-Bt	Bt	41	130	13.41	1.00	1.70	2.02	2.98	0.51	74.4	958	40.9	11	Bt	38.4	77.7		
TM-WB-4-A	A	42	50	13.05	0.70	1.60	1.49	2.81	0.50	77.0		36.0						
TM-FB-1-C	C	59	185*	9.30	10.85	1.29	4.00	1.92	0.37	29.8		76.2						
TM-FB-1-Bkt1	Bkt	59	75*	14.02	2.41	1.46	2.89	3.24	0.55	67.4	834	49.6						
TM-FB-1-Bkt2	Bkt	60	25*	13.16	5.27	1.34	4.23	2.93	0.53	52.8		62.9						
TM-WB-13-Bt	Bt	63	70	13.06	1.08	1.53	2.17	3.09	0.49	74.5	959	41.4	11					
TM-HC-14-Bt	Bt	67	75	12.25	8.94	0.50	7.58	2.64	0.55	41.8	503	82.8						
TM-FB-7-Bt	Bt	72	110	13.26	0.80	1.43	2.02	2.97	0.50	77.7	1022	38.4	11					
TB-FB-11-Bkt	Bkt	89	75	14.02	4.13	0.92	3.29	4.28	0.53	60.8		60.1						
										Mean MAP (mm yr^{-1})[a]	*860 ± 200*	*MAAT (°C)[a]*	*11 ± 2*					

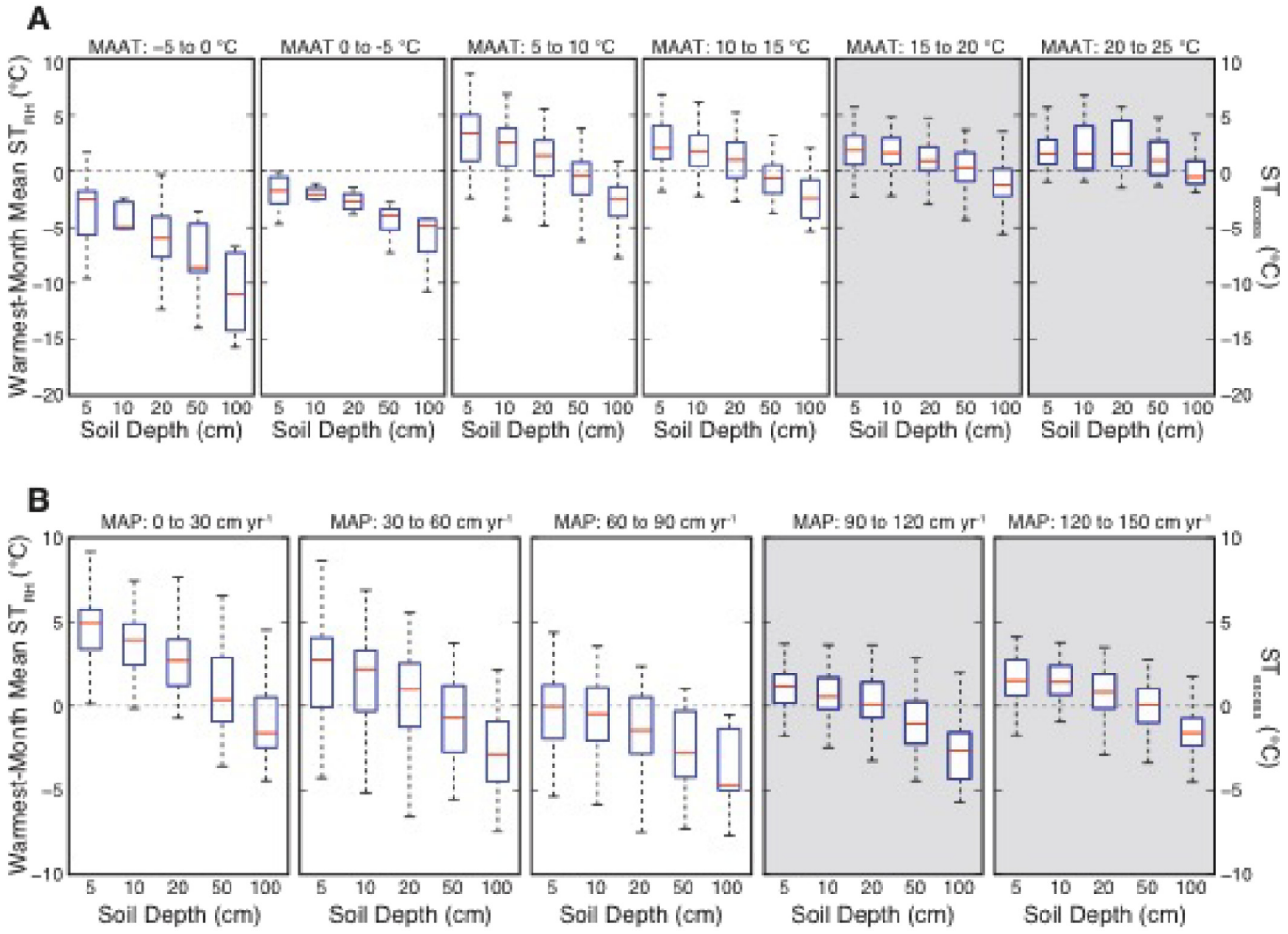

Fig. 7. Soil excess temperatures from incident solar radiative heating (ST_{RH}) calculated from SCAN station (n = 205 stations) soil and air temperature data binned by: A) mean annual temperature (MAAT) and B) mean annual precipitation (MAP) at soil depths from 5 to 100 cm. In both A and B, the gray boxes indicate the MAAT and MAP conditions most similar to the climate conditions of the KF and TMF during the Late Cretaceous. Red lines represent median values for each bin, while blue boxes indicate 2σ and vertical dashed lines indicate full range of values. Horizontal dashed line indicates an ST_{RH} value of 0 °C (i.e., identical soil and air temperatures). (For interpretation of the references to color in this figure legend, the reader is referred to the web version of this article.)

(Niezgodzki et al., 2017). To put these summer temperatures in perspective, climate reanalysis data (ERA-Interim) shows that currently, < 8% of the Earth's surface experiences warmest month mean air temperatures ≥35 °C, and these areas are restricted to arid and semi-arid regions in the sub-tropics (e.g., North Africa, the Middle East, and parts of the Indian subcontinent).

5.2. Soil geochemistry estimates of MAAT and MAP compared to previous reconstructions

Geochemistry-based paleosol proxies of MAAT and MAP, such as PWI and CIA−K, have proven challenging to apply to certain soil types because they can be compromised by a variety of factors such as high sediment accumulation rates, insufficient soil development, and inappropriate application to certain soil classes. For example, the CALMAG proxy, which was developed by Nordt and Driese (2010) to reconstruct MAP for Vertisols cannot be applied to the Alfisols and Inceptisols described in this study. A comparison of our PWI and CIA-K values for the KF and TMF shows that they underestimate MAAT and MAP relative to previous estimates and model simulations (e.g., Sewall and Fricke, 2013) and suggests that they are inappropriate for use in calculating MART for our study sites. For both the KF and TMF, the mean PWI MAAT values underestimate other proxy reconstructions by ~7 to 11 °C for the KF and ~3 to 8 °C for the TMF (Table 5; Upchurch et al., 2015; Miller et al., 2013; Barrick et al., 1999; Van Boskirk, 1998; Wolfe, 1990; Wolfe and Upchurch, 1987). Likewise, CIA-K MAP predictions for the KF are roughly half the 1780 mm yr $^{-1}$ predicted from fossil leaf size (Miller et al., 2013). MAP estimates for the TMF are less well constrained, but our CIA-K estimates are at the lower end of the range of estimated values from fossil leaves (900 to 1200 mm yr^{-1}; Falcon-Lang, 2003). Gallagher and Sheldon (2013) note that high abundance of Ca in a Bt horizon will result in artificially low PWI-based MAT estimates. However, except for one Bt horizon from the KF, our paleosol Bt horizons have relatively low Ca abundances, suggesting that some other factor(s) is affecting paleoclimate estimates based on the Bt horizon geochemistry.

We suggest that three factors influenced the KF and TMF soils during formation, leading to higher (lower) PWI (CIA−K) values and unrealistically low MAT and MAP estimates. First, the extremely high sediment accumulation rates during deposition of the KF (39 to 41 cm ka^{-1}; Roberts et al., 2005) may have provided a nearly continuous supply of fresh sedimentary material to the forming soils. If this input of fresh material (and the associated cations used to calculate PWI and CIA−K: Al, Ca, K, Mg, and Na) kept pace with soil weathering and leaching, the resulting PWI and CIA-K values would not reflect local MAT and MAP. Second, due to the high sedimentation rates described above, the KF paleosols may have simply been too weakly developed to have achieved geochemical equilibrium with their environment

Table 5
Mean annual air temperature reconstructions for the Kaiparowits (KF) and Two Medicine (TMF) Formations.

Formation	Paleolatitude (°N)[a]	Distance from KF or TMF (°)[b]	Age	Proxy	MAAT (*C)[c]	Latitude-adjusted MAT (*C)[d]		Uncertainty (± °C)	Reference	Notes
						High	Low			
MAAT estimates for the Kaiparowits Formation										
Kaiparowits	46.2	0	Upper Campanian	LMA	20	20	20	2	Miller et al., 2013	
Vermejo	43.6	− 2.6	Upper Campanian/ Lower Maastrichtian	CLAMP	18	17	17	1	Wolfe, 1990	
McRae	42.0	− 4.2	Upper Campanian/ Lower Maastrichtian	LMA	22	21	20	2	Upchurch et al., 2015	
MAAT estimates for the Two Medicine Formation										
Two Medicine	55.0	0	Campanian	LMA	16	16	16	5	Foreman et al., 2011; Falcon-Lang, 2003; Wolfe and Upchurch, 1987	Based on the Late Cretaceous latitudinal temperature gradient reconstructed by Wolfe and Upchurch (1987) from multiple North American fossil leaf assemblages using leaf margin analysis. Uncertainty from Peppe et al. (2011)
Judith River	55.6	0.6	Upper Campanian	Turtle and Gar $\delta^{18}O$	14	14	14	1	Barrick et al., 1999	Late Cretaceous river temperature.
Judith River	55.6	0.6	Upper Campanian	Turtle and Gar $\delta^{18}O$	16	17	17	1	Barrick et al., 1999	Late Cretaceous river temperature.
Judith River	55.6	0.6	Upper Campanian	Turtle and Gar $\delta^{18}O$	19	19	19	1	Barrick et al., 1999	Late Cretaceous river temperature.
Eagle	50.9	− 4.05	Lower Campanian	LMA	16	15	14	5	Van Boskirk, 1998	Uncertainty from Peppe et al. (2011)

[a] Paleolatitudes from Upchurch et al. (2015) and Miller et al. (2013).
[b] Calculated as straight-line north or south distance from the KF and TMF in degrees of latitude.
[c] Mean annual air temperature (MAAT).
[d] The latitude adjusted MAAT values for the KF and TMF were calculated using the Wolfe and Upchurch (1987) Late Cretaceous North American latitudinal temperature gradient of 0.3 to 0.4 °C.

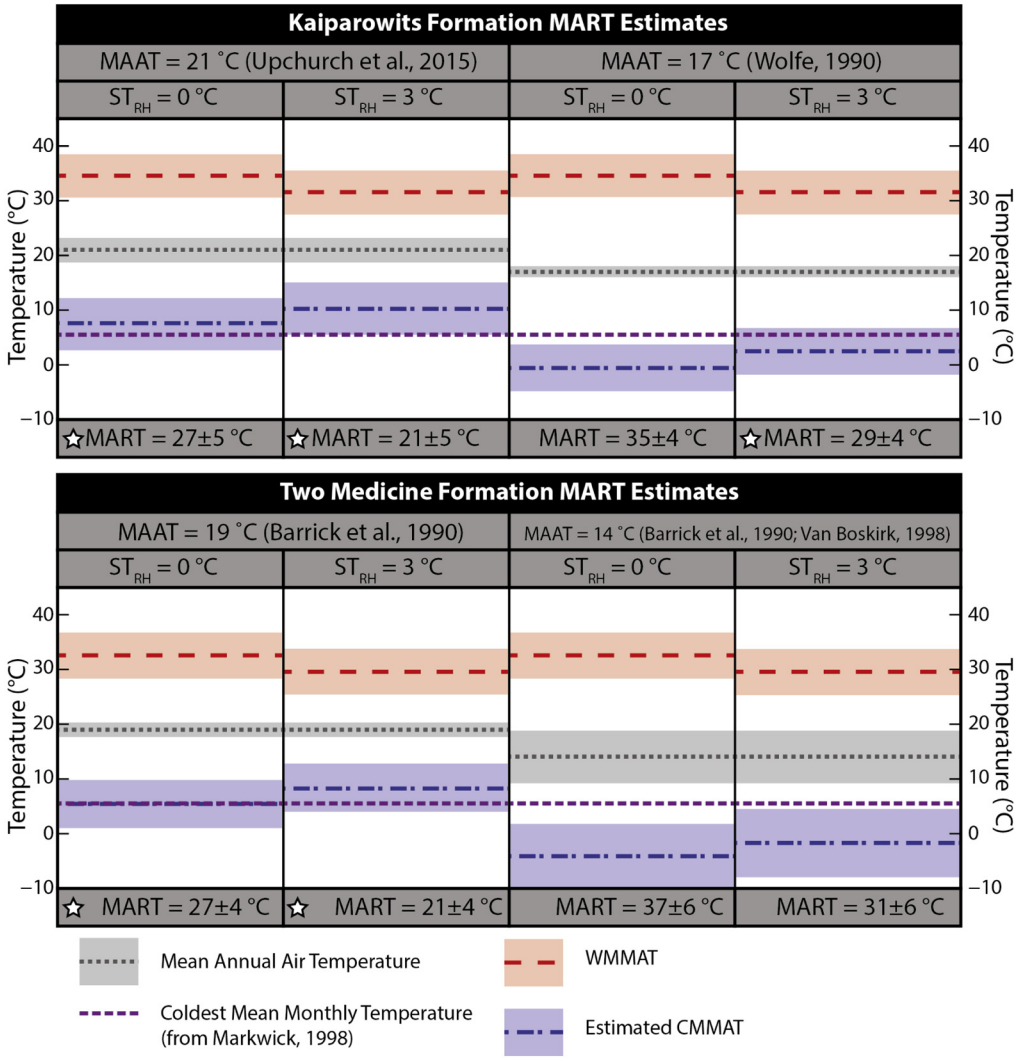

Fig. 8. Mean annual range in temperature (MART) for the KF (upper panel) and TMF (lower panel). Winter cold temperature limit (purple small dashed line) estimated from the presence of fossil crocodilians (Markwick, 1998). Previous MAAT estimates for the KF and TMF from LMA, CLAMP and vertebrate fossil $\delta^{18}O$ denoted by the gray dotted line. Warmest month mean soil temperature reconstructed from paleosol carbonate T(Δ_{47}) (red large dashed line) calculated assuming an STRH of either 0 °C or 3 °C. Estimated coldest mean month temperature denoted with blue dot-dashed line. White stars indicate the favored MART estimates that produce CMMT values consistent with the presence of fossils crocodilians in the KF and TMF. (For interpretation of the references to color in this figure legend, the reader is referred to the web version of this article.)

(Stinchcomb et al., 2016). Third, many of the paleosols in both the KF (58%) and TMF (30%) display vertic features such as well-developed slickensides and distinct clay accumulations. While these features are not developed enough to classify these soils as Vertisols, Buol et al. (2011) note that the presence of such features in other soil types inhibits the leaching of cations from the soil, which would in turn result in high (low) PWI (CIA-K) values and unrealistically low MAT and MAP estimates.

Based on these considerations, we attribute the high (low) PWI (CIA−K) values from our paleosols to physical processes such as sediment deposition rates and soil structural features rather than climate-dependent weathering conditions. Because of this, we choose to calculate MART based on previous estimates of MAT from the KF and TMF (see Section 2.1). In order to provide a range of possible MART values we utilize latitude-adjusted MAT reconstructions from formations that formed coevally with, and in close proximity to, our study areas, and that represented similar alluvial or coastal plain settings along the WIS (see Table 5 and the online Supplementary Information; Upchurch et al., 2015; Barrick et al., 1999; Van Boskirk, 1998; Wolfe, 1990). The MART estimates that result from using these ranges of MAT reconstructions are discussed in the following section.

5.3. Calculating Late Cretaceous MART and cold month mean air temperature

Modern MART is calculated by subtracting local winter temperatures from local summer temperatures (Peppe et al., 2011; Bailey, 1966); however, because quantitative winter temperature estimates are unavailable for the KF and TMF, we calculate Late Cretaceous MART as twice the difference between warm month mean air temperature (from our paleosol T(Δ_{47}) values) and MAAT from previous paleobotanical (Upchurch et al., 2015; Miller et al., 2013; Van Boskirk, 1998; Wolfe and Upchurch, 1987) and fossil phosphate oxygen isotope reconstructions (Barrick et al., 1999). The use of paleobotanical MAAT reconstructions is justified for two reasons: 1) LMA and CLAMP reconstructions of MAAT are considered more robust than paleobotanical reconstructions of warmest and coldest month mean temperatures (see Section 2.2 and Jordan et al., 1996, Jordan, 1997); and 2) for both the KF and TMF, we estimate the range in MAAT from at least two studies using different proxy methods. In order to take into account the possible uncertainties associated with our various assumptions, we calculate four different MART and cold month mean air temperature values for each study area. First, we make use of the warmest and coldest MAAT estimates available for the KF and TMF formations, or for coeval formations in close proximity (Table 5), which provides a window of possible MAAT values. MAAT estimates for the various formations listed in Table 5 were adjusted based on the north/south latitudinal distance between the given formation and the KF or TMF, and the predicted Late Cretaceous latitudinal temperature gradient (0.3 to 0.4 °C °latitude^{-1}; Amiot et al., 2004; Wolfe and Upchurch, 1987). All of the formations used for these MAAT estimates come from coeval, low elevation, coastal or alluvial plain depositional environments along the

WIS (Miller et al., 2013; Foreman et al., 2011; Barrick et al., 1999; Van Boskirk, 1998; Wolfe, 1990; Lozinsky et al., 1984). For example, Upchurch et al. (2015) reported a MAT of 22 °C for the late Campanian/early Maastrichtian McCrae Formation in southwestern New Mexico, which is located 4.2° south of the KF. Thus, the adjusted MAT for the KF based on the Upchurch et al. (2015) MAAT reconstruction is 21 to 20 °C, consistent with the Miller et al. (2013) MAT estimate for the KF. We note that the latitudinal corrections made here are generally smaller than the uncertainty reported for the MAAT estimates, suggesting that these corrections are not a significant source of bias. Second, we assume two different values of warm month mean air temperature: first, we calculate MART and cold month mean air temperature assuming there is no radiative soil heating, such that warmest month mean air temperature is equal to warmest month mean soil temperature (e.g., our mean T(Δ_{47}) values); second, we perform the same calculations, but we assume a maximum ST_{RH} value by subtracting 3 °C from our T(Δ_{47}) values. For each of these calculations there are three sources of quantifiable uncertainty: 1) the mean analytical uncertainty of the sample T(Δ_{47}) estimates (± 1 SE = 4 °C for both the KF and TMF samples); 2) the uncertainty on the mean of the KF and TMF samples (± 2 and ± 4 °C, respectively); and 3) the analytical uncertainty of the MAAT estimates from each site, as reported in Table 5.

The initial MART estimates for the KF range from 21 ± 5 to 35 ± 4 °C, and from 21 ± 4 to 37 ± 6 °C for the TMF (Fig. 8; Table 6). Coldest month mean air temperature estimates based on these MART values are −1 ± 4 to 10 ± 5 °C for the KF, and − 5 ± 6 to 8 ± 4 °C for the TMF. As discussed in Section 2.2, the presence of crocodilian fossils in both the KF (e.g., Farke et al., 2014; Boyd et al., 2013; Getty et al., 2010) and TMF (e.g., Horner et al., 2001; Varricchio, 1995) place a lower limit of ~5 °C (Markwick, 1998) on long-term coldest month mean air temperature. If this temperature tolerance was conserved in Cretaceous crocodilians, it would indicate that our lowest coldest month mean air temperature estimates for the KF (−1 ± 4 °C) and the lowest two estimates for the TMF (−5 ± 6 and −2 ± 6 °C) are likely too cold. This suggests that the best estimate of coldest month mean air temperature for the KF is ~2 to ~10 °C, and ~5 to ~8 °C for the TMF.

Ruling out those MART reconstructions that result in coldest month mean air temperature estimates below 5 °C leads to a narrower range of ~21 to ~29 °C for the KF MART values, and ~21 to ~27 °C for the TM MART values. Because our review of SCAN station soil and air temperature data shows that ST_{RH} values of 3 °C or higher are extremely rare in humid environments, we suggest that the high end of our range of MART estimates are the most plausible, since they assume no radiative soil heating.

The MART estimates for the KF and TMF are significantly larger than past reconstructions derived mainly from leaf physiognomy proxies (MART = 8 to 10 °C; Hunter et al., 2013; Wolfe and Upchurch, 1987), and suggest that mid-latitude seasonal temperature changes during the Late Cretaceous were of similar magnitudes to modern mid-latitude sites. The smaller MART estimates from leaf physiognomy could be due to the inaccuracies in warmest and coldest month temperature estimates from CLAMP and other leaf physiognomy proxies capable of reconstructing seasonal temperatures, as described by previous studies (e.g., Spicer et al., 2004, Jordan et al., 1996, Jordan, 1997). Such inaccuracies can be caused by a variety of climate, biologic, and geologic processes, including: 1) taphonomic loss of leaf physiognomic characters (Spicer et al., 2005); 2) evapotranspiration cooling of forest canopies (Spicer et al., 2011); 3) the weak relationship between leaf size and warmest mean monthly temperature (Spicer and Yang, 2010); 4) high regional dependence of warmest and coldest month mean temperatures; or 5) covariance between warmest and coldest month mean temperatures, and a lack of independence between seasonal temperatures and MAAT (Jordan et al., 1996; Jordan, 1997).

5.4. Evaluating paleosol carbonate T(Δ_{47}) MART reconstructions

In order to further evaluate the uncertainties associated with these MART reconstructions, we use ERA-Interim climate reanalysis data to 1) test our basic assumption that the annual distribution of temperatures is symmetrical about MAAT; and 2) compare modern MART estimates calculated first as the difference between modern warmest month mean air temperature and coldest month mean air temperature (hereafter referred to as $MART_{S\text{-}W}$), and second—following our method for calculating Late Cretaceous MART—as twice the difference between warmest month mean air temperature and MAAT ($MART_{S\text{-}MAT}$).

For most low- and mid-latitude environments, our assumption that annual temperatures are distributed symmetrically about local MAAT holds true. We tested this assumption by calculating latitudinal changes in seasonal asymmetry for a variety of terrestrial land cover types identified from the MODIS land cover dataset. For the purposes of this paper we define seasonal asymmetry as the difference between WMMT and MAAT minus the absolute value of the difference between CMMT and MAAT. For this calculation, MAAT is specifically calculated as the mean of monthly mean temperatures. Following this definition, a location with a seasonal asymmetry value of 0 °C would have a symmetrical (i.e., normal) distribution of temperatures about MAAT. In contrast, sites with positive seasonal asymmetry values have annual temperature distributions that are skewed towards CMMT, and sites with negative seasonal asymmetry values have temperature

Table 6
Mean annual, warmest mean month, coldest mean month, and mean annual range in temperature results.

MAAT estimate (°C)[a]	± 1 SE (°C)	Reference	ST_{RH} (°C)	WMMAT (°C)[b]	± 1 SE (°C)	CMMAT (°C)[c]	± 1 SE (°C)	MART (°C)[d]	± 1 SE (°C)
Kaiparowits Formation									
21	2	Upchurch et al., 2015	0	35	4	7	5	27	5
21	2	Upchurch et al., 2015	3	32	4	10	5	21	5
17	1	Wolfe, 1990	0	35	4	−1	4	35	4
17	1	Wolfe, 1990	3	32	4	2	4	29	4
Two Medicine Formation									
19	1	Barrick et al., 1990	0	33	4	5	4	27	4
19	1	Barrick et al., 1990	3	30	4	8	4	21	4
14	5	Barrick et al., 1990; Van Boskirk, 1998	0	33	4	−5	6	37	6
14	5	Barrick et al., 1990; Van Boskirk, 1998	3	30	4	−2	6	31	6

[a] Mean annual air temperature (MAAT).
[b] Warmest month mean air temperature (WMMAT). Lower WMMAT values calculated by subtracting 3 °C from the mean paleosol carbonate T(Δ_{47}) results in order to account for maximum radiative soil heating.
[c] Coldest month mean air temperature (CMMAT). Italicized values are interpreted as too cold to be reasonable based on the presence of crocodilian fossils in both the Kaiparowits and Two Medicine Formations.
[d] Mean annual range in temperature (MART). Italicized values are interpreted as too cold to be reasonable based on the presence of crocodilian fossils in both the Kaiparowits and Two Medicine Formations.

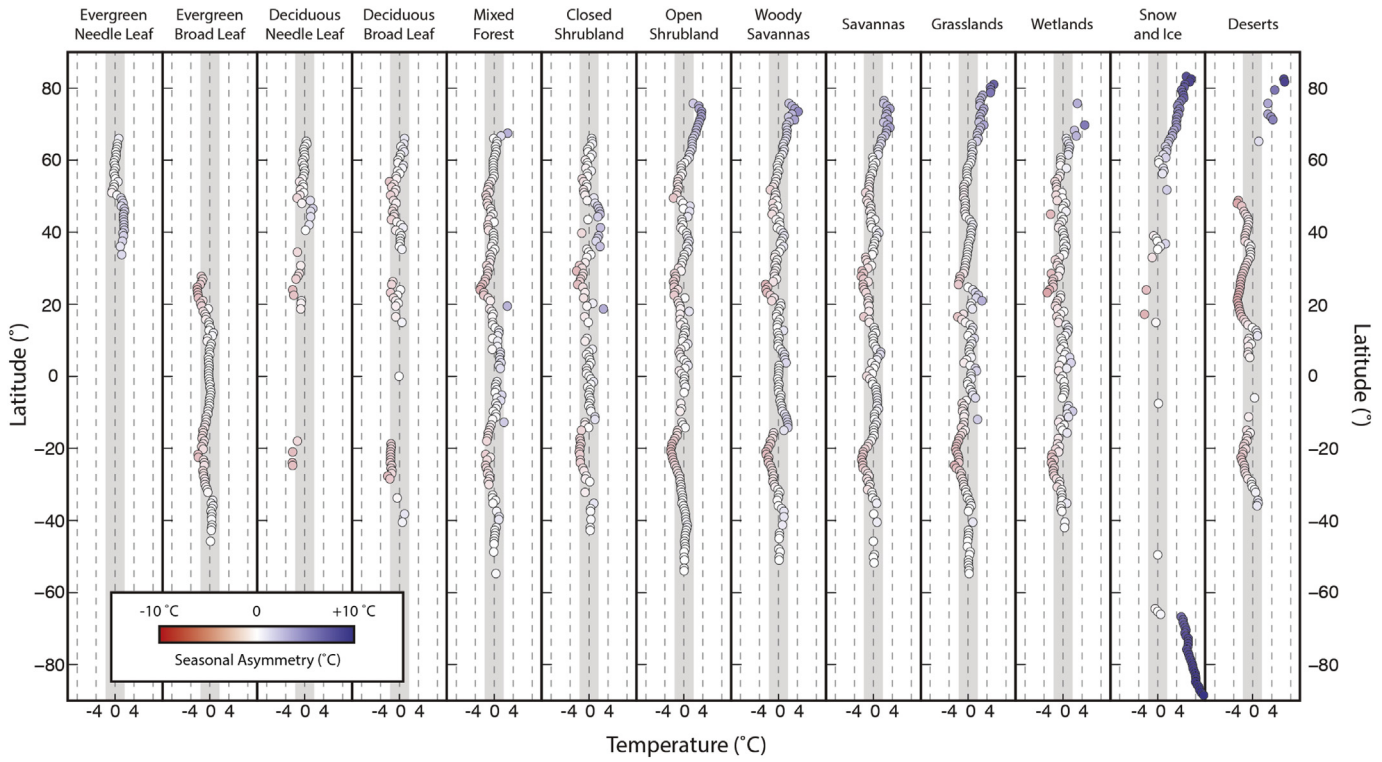

Fig. 9. Seasonal asymmetry calculated for thirteen different terrestrial biomes by latitude using ERA-Interim climate reanalysis data. A seasonal asymmetry value of 0 °C indicates that the annual distribution of air temperatures is symmetrical about local MAAT. In contrast, seasonal asymmetry values > 0 °C shows that the annual distribution of air temperatures is skewed towards the winter season, and values < 0 °C shows that temperatures are skewed towards the summer season. Note that all of the biomes present at high latitudes show increasingly positive seasonal asymmetry values, while the most negative seasonal asymmetry values are found in the subtropics (mainly in deserts). The vertical gray bands show the minimum uncertainty associated with carbonate clumped isotope thermometry (seasonal asymmetry values within this band would not be distinguishable from a seasonal asymmetry value of 0 °C. This data suggests that for most mid-latitude environments where paleosol carbonates are likely to be preserved, the distribution of temperatures about MAAT is symmetrical.

Table 7
Latitudinal trends in seasonal asymmetry values[a] for thirteen different land cover types[b].

Latitude (°)	Evergreen Needle Leaf	Evergreen Broad Leaf	Deciduous Needle Leaf	Deciduous Broad Leaf	Mixed Forest	Closed Shrubland	Open Shrubland	Woody Savannas	Savannas	Grasslands	Wetlands	Snow and Ice	Deserts
90 to 80	–	–	–	–	–	–	–	–	–	5.02	–	6.20	6.69
80 to 70	–	–	–	–	–	–	3.29	2.90	2.70	3.01	3.02	4.61	3.89
70 to 60	0.39	–	0.07	0.64	0.65	0.30	1.98	1.29	1.80	1.62	1.55	2.51	1.32
60 to 50	−0.09	–	−0.41	−0.66	−0.62	−0.63	−0.76	−0.51	−0.54	−0.30	−0.82	0.96	–
50 to 40	1.74	–	0.56	−0.81	−0.98	1.44	−0.12	−0.45	−0.52	−0.16	−0.39	–	−1.61
40 to 30	1.51	–	−1.16	0.22	−0.50	0.25	0.42	0.20	−0.15	−0.01	−0.18	−0.04	−0.98
30 to 20	–	−2.11	−1.52	−0.92	−1.82	−1.39	−1.47	−1.31	−1.73	−0.03	−1.62	−2.42	−2.56
20 to 10	–	−0.45	−0.78	−0.34	0.22	0.21	−0.16	0.03	−0.49	0.00	−0.19	−1.62	−1.19
10 to 0	–	−0.15	–	–	0.97	−0.14	−0.14	0.50	0.37	0.49	0.23	–	−0.76
0 to −10	–	−0.08	–	−0.08	0.55	0.22	−0.11	0.25	0.35	0.04	0.46	0.17	0.46
−10 to −20	–	−1.17	−1.55	−1.72	−0.51	−0.82	−1.33	0.18	−0.04	−1.17	−0.17	–	−1.19
−20 to −30	–	−1.48	−2.53	−1.85	−1.34	−1.31	−1.78	−1.79	−1.84	−2.00	−1.80	–	−1.63
−30 to −40	–	0.07	–	0.32	0.11	0.25	−0.16	0.08	−0.25	−0.12	−0.34	–	0.62
−40 to −50	–	0.33	–	0.64	0.11	0.25	0.37	0.26	0.31	0.18	0.38	−0.05	–
−50 to −60	–	–	–	–	0.33	–	0.09	0.12	0.06	0.10	–	–	–
−60 to −70	–	–	–	–	–	–	–	–	–	–	–	3.37	–
−70 to −80	–	–	–	–	–	–	–	–	–	–	–	6.40	–
−80 to −90	–	–	–	–	–	–	–	–	–	–	–	8.38	–

[a] Temperatire data from the ERA-Interim climate reanalysis project (Dee et al., 2011).
[b] Land cover data from MODIS imagery (Channan et al., 2014; Friedl et al., 2010).

distributions skewed towards WMMT. Fig. 9 and Table 7 show that for all low- and mid-latitude land cover types except ice-covered terrain and deserts, seasonal asymmetry is small (μ = −0.3 ± 1.2 °C). In contrast, high latitude sites (latitude > 60 °N/°S) show much larger seasonal asymmetry values (μ = 4.0 ± 2.1 °C), regardless of the land cover type. Finally, deserts show distinct negative seasonal asymmetry trends in the sub-tropics (see Fig. 9). We suggest that the large seasonal asymmetry values calculated for high latitude sites may be due to a combination of the unique annual solar insolation pattern (prolonged summer light and winter darkness) as well as albedo effects associated with ice sheets and deserts. This observation aside, the seasonal asymmetry values presented above suggest that at low- and mid-latitudes, annual temperatures are typically distributed symmetrically about local MAAT, consistent with our assumption.

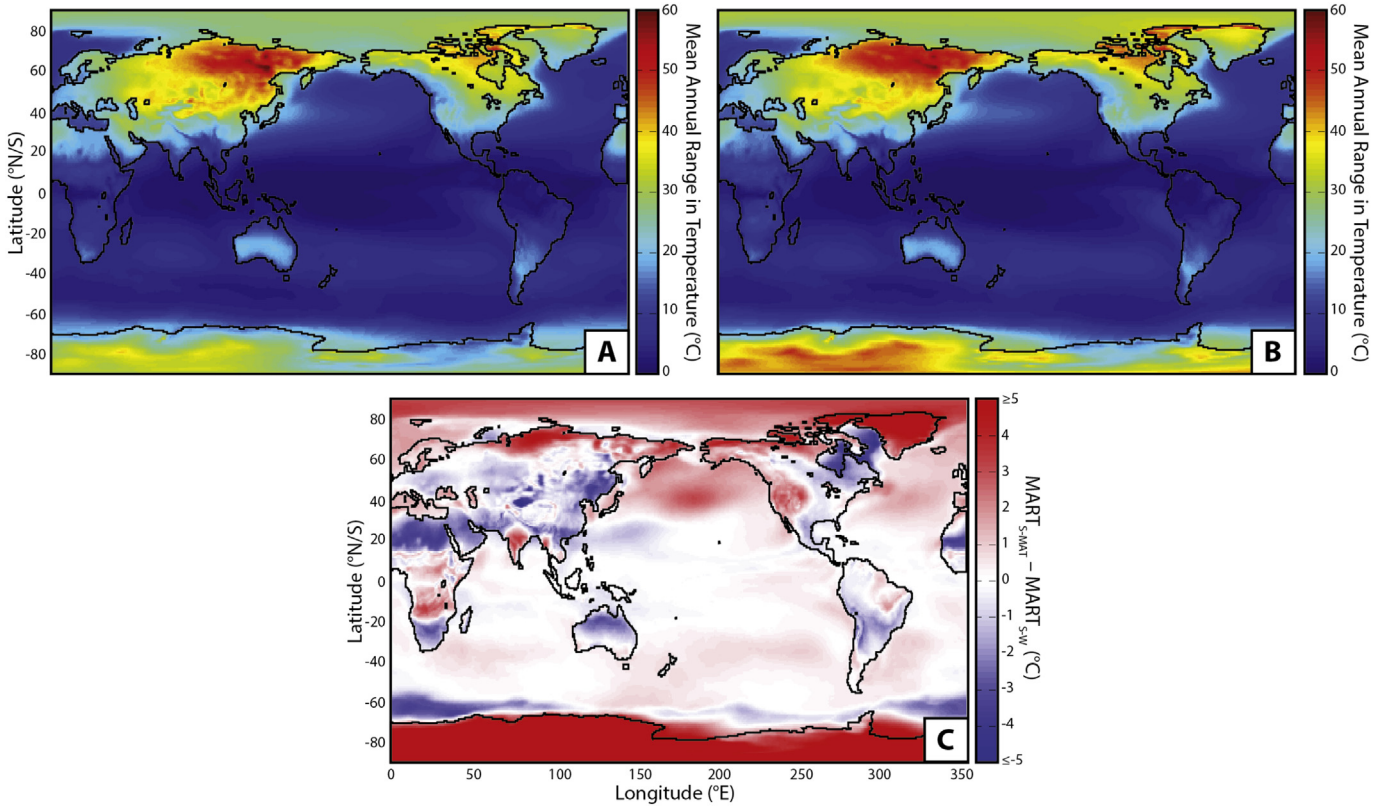

Fig. 10. Mean annual range in temperature (MART) calculations, based on: A) summer minus winter temperatures ($MART_{S\text{-}W}$), and B) twice the difference between summer and mean temperatures ($MART_{S\text{-}MAT}$). Panel C shows the temperature difference between $MART_{S\text{-}MAT}$ and $MART_{S\text{-}W}$. Temperature data from ERA-Interim reanalysis output.

These constraints on the degree of seasonal asymmetry in different environments suggest small effect on the accuracy of our paleo-MART reconstructions. As shown in Fig. 10, the two different methods of calculating MART (i.e., WMMT minus CMMT versus twice the difference between WMMT and MAAT) produce very similar results, especially at for the mid-latitudes. The mean effect of calculating MART as twice the difference between WMMT and MAAT is −0.03 °C, with a max and min of 3.60 and − 5.05 °C residual from MART calculated from summer-winter, respectively. We attribute the larger differences between the two methods of calculating MART at high latitude to the higher seasonal asymmetry these sites experience. These findings suggest that calculating MART from just warmest month mean air temperature and MAAT should produce accurate estimates of the actual range in seasonal temperatures for nearly all mid-latitude terrestrial environments, providing additional confidence that our Late Cretaceous MART calculations are accurately capturing the true range in seasonal temperatures.

We note that the potential error on our MART estimates is non-trivial (± 4 to 6 °C) despite careful screening and a large number replicate carbonate analyses. In view of this fact, we suggest that future MART reconstruction studies will benefit from both a larger number of samples and replicate measurements than is traditionally collected for paleosol carbonate studies, and from the recalculation of older MAAT estimates from LMA (e.g., those presented in Wolfe and Upchurch (1987) and used in Foreman et al. (2011) and this study) using modern methods (see Peppe et al., 2011) to reduce associated uncertainties.

5.5. Implications for seasonality in greenhouse climates

Having calculated Late Cretaceous MART values and evaluated their accuracy and uncertainties, we now compare the reconstructed MARTs to modern seasonal variability. This can be challenging because there are no perfect modern analogs for our study areas due to the fact that modern locations with similar MAAT and MAP (e.g., the Gulf Coast of the United States; Miller et al., 2013) are restricted to much lower latitudes than the Late Cretaceous paleolatitudes of the KF and TMF, and no major interior seaways exist in the modern. However, a comparison of our Late Cretaceous MART results to a suite of modern MART values shows that our estimates are consistent with the range of MART seen in North America today (Fig. 11). In the modern, MARTs between 45 and 55 °N (the approximate paleolatitude of the KF and TMF) are highly variable. Globally, mean MART calculated from ERA-Interim climate reanalysis data at 55 °N/S is 31 °C, while the mean North American MART at the same latitude is 28 °C and the mean MART at the modern longitude of the KF and TMF formations is just 23 °C. This range of MART values is consistent with our range of KF reconstructions; however, the TMF MART reconstructions are more consistent with the lower MART values calculated at the same longitude (248 °E) as the modern study site (red line in Fig. 11). Lower-latitude environments like the Gulf Coast–despite being similar to the KF in terms of temperature and precipitation (Miller et al., 2013; Tidwell et al., 2007)–experience significantly lower MART than our reconstructions due to their lower latitude positions. These findings may suggest that latitude and elevation has a larger impact on terrestrial seasonality than global mean surface temperatures, regardless of whether the climate is in a greenhouse or icehouse state (Sloan and Barron, 1990).

In addition to a comparison against modern MART values, we evaluate our KF and TMF MART, warmest month mean air temperature, and coldest month mean temperature estimates against MART values calculated from Late Cretaceous climate model output generated by Sewall and Fricke (2013). Due to differences in the longitudinal position of the paleogeographic reconstructions used in this study versus the reconstruction used in the Sewall and Fricke (2013) model, we compare our results to the output from three model grid cells located

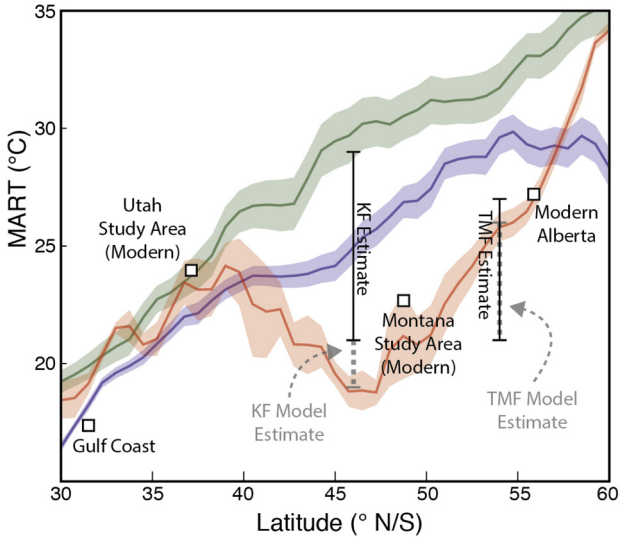

Fig. 11. Mean annual range in temperature (MART) versus latitude. The green line and band show global mean MART at the 95% confidence interval, the blue line and band show North American mean MART at the 95% confidence interval, and the red line and band show mean MART at the longitude of the KF and TMF study sties. Note that the variability in MART along the longitude of the study sites is mainly due to variability in topography, since the transect passes over the Colorado Plateau and the eastern edge of the Rocky Mountains. Black error bars show MART reconstructions for the KF and TMF and the thick gray dashed bars are the simulated MART for the KF and TMF using model output from Sewall and Fricke (2013) and their reconstructed paleolatitudes (Miller et al., 2013). White squares show modern MART values for various related locations. (For interpretation of the references to color in this figure legend, the reader is referred to the web version of this article.)

around the KF study area, and four model grid cells around the TMF study area. Grid cells were chosen to avoid cooler upland and ocean areas (Fig. 12). The mean model estimates of coldest month mean air temperatures for the KF study area are 3 °C warmer than our reconstructions, but our TMF coldest month mean air temperature estimates agree well with modeled winter temperatures, regardless of the exact MAAT and ST_{RH} values used in our MART calculations. The model underestimates warmest month mean temperature relative to our proxy reconstructions by ~4 °C at both sites—a common issue with model simulations of both the Late Cretaceous and Eocene greenhouse periods (Snell et al., 2013; Spicer et al., 2008). Calculations of MART using the model output yield mean values of 20 ± 2 and 23 ± 2 °C for the KF and TMF, respectively. The model MART estimates for the KF are consistent with the lower limits of our KF MART reconstructions, while the model MART estimates and our MART reconstructions for the TMF are in very good agreement.

We interpret the minor differences between the model simulations and our proxy reconstructions and estimates to be the result of some combination of: 1) spatial averaging of warmest and coldest month mean air temperatures due to the relatively coarse model resolution (~2.8° latitude × 2.8° longitude; Sewall and Sloan, 2006); 2) the accidental inclusion of cooler upland regions in estimates of average model temperatures; and 3) uncertainty in the exact location of the KF and TMF study sites relative to the model grid due to differing paleogeographic reconstructions. We note that in addition to being consistent with the Sewall and Fricke (2013) simulation of Late Cretaceous North America, our results are in general agreement with past global or other regional modeling studies suggestive of a modern range in seasonality during the Late Cretaceous and other greenhouse periods (e.g., Hunter et al., 2013; Huber and Caballero, 2011; Valdes, 2011; Spicer et al., 2008; Deconto et al., 1999).

Our Late Cretaceous MART reconstructions add to a growing body of proxy evidence suggesting that terrestrial environments experience

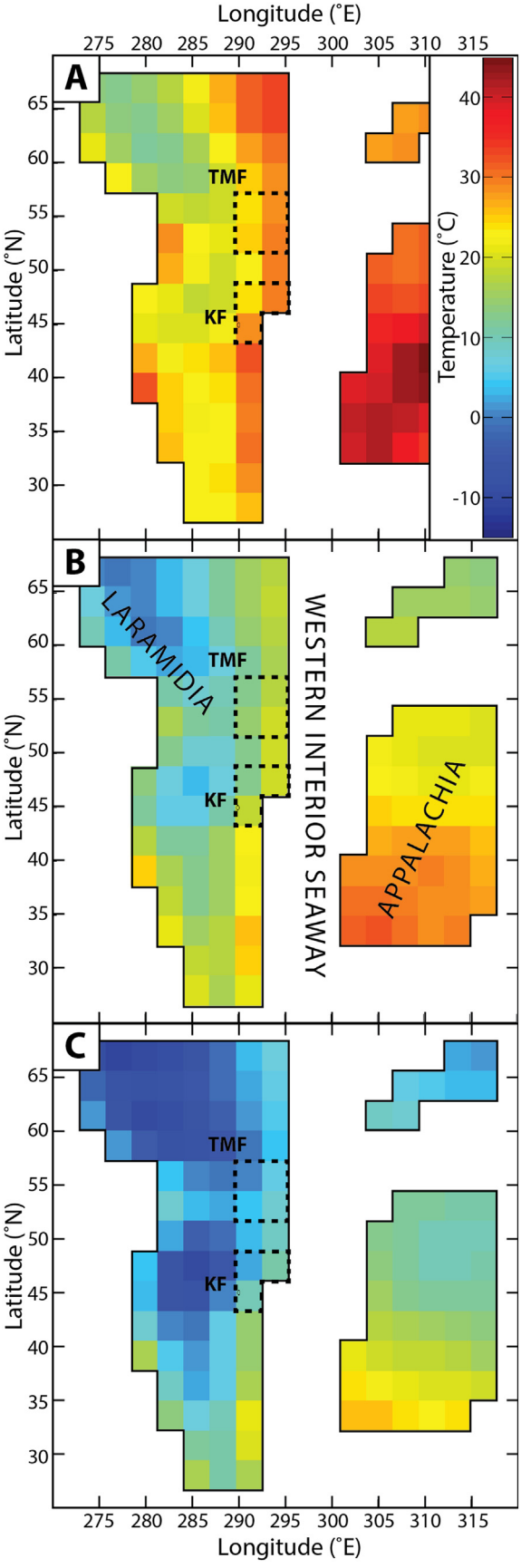

(caption on next page)

Fig. 12. Visualization of Sewall and Fricke (2013) Late Cretaceous (Campanian) global climate model output. The grid cells used for comparison with our Kaiparowits (KF) and Two Medicine Formation (TMF) paleoclimate reconstructions are highlighted with dashed black lines. Panel A shows warmest mean monthly air temperatures (WMMAT), panel B shows mean annual air temperatures (MAAT), and panel C shows coldest mean monthly air temperatures (CMMAT). Additional text in panel B provides the name of relevant paleogeographic locations.

similar magnitudes of seasonal temperature change in both greenhouse and icehouse conditions (Hyland et al., 2018; Kelson et al., 2018; Suarez et al., 2017; Snell et al., 2013). Additionally, our results provide evidence that during greenhouse periods like the Late Cretaceous and Paleogene, MAAT is shifted to higher values, but MART remains essentially unchanged. Our MART reconstructions are similar in magnitude to model MART simulations (Sewall and Fricke, 2013; Snell et al., 2013; Sloan and Barron, 1990), which may indicate that disagreements between model simulations and proxy reconstructions of MART are likely due primarily to proxy shortcomings such as: 1) the effect of non-climate factors on leaf physiognomy proxies (e.g. Peppe et al., 2011), and 2) uncertainties regarding the climatic constraints of fossil plants and animals that are used as qualitative paleoclimate proxies. We note that uncertainties in model paleogeographic reconstructions may also limit the accuracy of proxy-model comparison studies (Kelson et al., 2018).

The presence of modern-magnitudes of MART in the Late Cretaceous also has implications for the geographic distribution and lifestyles of dinosaur and non-dinosaur faunal communities in western North America, and our understanding of vertebrate speciation patterns. There has been a long-standing debate regarding the degree of provincialism (regional partitioning) of northern and southern faunal communities along the western margin of the WIS during the Late Cretaceous (e.g., Leslie et al., 2018; Lucas et al., 2016; Morrone, 2014; Nydam et al., 2013; Gates et al., 2010; Sampson et al., 2010; Lehman et al., 2006; Lehman, 2001). Faced with a lack of known geographic barriers to animal migration, studies in favor of faunal provincialism have often cited latitudinal changes to unspecified climate parameters (e.g., temperature and/or precipitation) as the driving force behind regionally discrete animal populations (e.g., Gates et al., 2010; Sampson et al., 2010). The approximate latitudinal position of this climate interface between the northern and southern provinces has been speculated to be near the present day northern borders of Utah and Colorado (Sampson et al., 2010), placing it between our two study areas. However, when paired with previous estimates of MAAT for both the KF and TMF, our warmest month mean temperature, MART, and coldest month mean temperature reconstructions indicate that environmental conditions were similar in southern Utah and northwestern Montana during deposition of the KF and TMF, with only slightly cooler conditions characterizing the TMF during the winter. The difference in MAAT between the two sites was $< 5\,^{\circ}C$, and MART was essentially identical. These findings suggest that there were no distinct MART-related environmental changes between the KF and TMF that would have promoted geographic partitioning of large terrestrial animals in western North America during the Late Cretaceous. This may suggest that if some sort of climate barrier did exist between the northern and southern provinces of the western margin of the WIS, it may have been related to changes in precipitation and/or water availability rather than changes in temperature (e.g., Fricke et al., 2010; Wolfe and Upchurch, 1987; Hallam, 1985, 1984; Parrish et al., 1982). Better quantitative constraints on the spatial variability of Late Cretaceous MAP and precipitation seasonality are needed to resolve this question.

6. Conclusions

Our findings show that Late Cretaceous MART along the mid-latitude region (paleolatitude: ~46 to 56 °N) of the western margin of the WIS was similar to mid-latitude MART in modern North America, and that no distinct change in MART or warmest and coldest month temperatures exists between the southern and northern limits of this area. Additionally, we show that: 1) reconstructing paleo-MART from warmest mean monthly temperatures and independent MAAT estimates should yield accurate results for most vegetated environments, and 2) in all but the driest environments, soil heating from incident solar radiation is typically $< < 3\,^{\circ}C$ (96% of SCAN stations) for commonly sampled soil types and depths (50–100 cm).

Using paleosol carbonate clumped isotope thermometry, modern-magnitude MARTs have now been reconstructed for both the Late Cretaceous and the Paleogene, suggesting that modeling efforts to simulate greenhouse climates are more accurate than has previously been argued, and increasing confidence in future predictions of MART under a range of climate change scenarios. Future studies of Late Cretaceous MART should focus on true continental interior environments and low-latitude sites to provide a more complete picture of how MART varied between different Late Cretaceous sites, as well as providing additional evidence for the limited effect of climate on faunal provincialism in North America during this period.

Acknowledgements

The authors acknowledge financial support from the Quaternary Research Center and laboratory support from the UW Isolab. We thank the Grand Staircase-Escalante National Monument staff for access to the Kaiparowits Formation outcrops in Utah, and Robert Wellman for access to the Two Medicine Formation outcrops in Montana. We thank Dr. Brady Foreman for his collegial review of the manuscript. The authors thank Dr. Katie Snell and an anonymous reviewer for their excellent comments and suggestions, and Dr. Thomas Algeo for his editorial support.

Appendix A. Supplementary data

Supplementary data to this article can be found online at https://doi.org/10.1016/j.palaeo.2018.12.004.

References

Amiot, R., Lécuyer, C., Buffetaut, E., Fluteau, F., Legendre, S., Martineau, F., 2004. Latitudinal temperature gradient during the Cretaceous Upper Campanian-Middle Maastrichtian: $\delta^{18}O$ record of continental vertebrates. Earth Planet. Sci. Lett. 226, 255–272. https://doi.org/10.1016/j.epsl.2004.07.015.

Bailey, H.P., 1966. The mean annual range and standard deviation as measures of dispersion of temperature around the annual mean. Geogr. Ann. Ser. A, Phys. Geogr. 48, 183–194.

Barrick, R.E., Fischer, A.G., Showers, W.J., 1999. Oxygen isotopes from turtle bone : applications for terrestrial paleoclimates? PALAIOS 14, 186–191.

Barron, E.J., 1983. A warm, equable cretaceous: the nature of the problem. Earth Sci. Rev. 19, 305–338. https://doi.org/10.1016/0012-8252(83)90001-6.

Barron, E.J., 1987. Eocene equator-to-pole surface temperatures: a significant climate problem? Paleoceanography 2, 729–739.

Barron, E.J., Fawcett, P.J., Peterson, W.H., Pollard, D., Thompson, S.L., 1995. Paleoceanography (October 10), 953–962.

Bartlett, M.G., Chapman, D.S., Harris, R.N., 2006. A decade of ground-air temperature tracking at emigrant pass observatory, Utah. J. Clim. 19, 3722–3731. https://doi.org/10.1175/JCLI3808.1.

Bernasconi, S.M., Müller, I.A., Bergmann, K.D., Breitenbach, S.F.M., Fernandez, A., Hodell, D.A., Jaggi, M., Meckler, A.N., Millan, I., Ziegler, M., 2018. Reducing uncertainties in carbonate clumped isotope analysis through consistent carbonate-based standardization. Geochem. Geophys. Geosyst. 19, 2895–2914. https://doi.org/10.1029/2017GC007385.

Berry, J., Bjorkman, O., 1980. Photosynthetic response and adaptation to temperature in higher plants. Annu. Rev. Plant Physiol. 31, 491–543. https://doi.org/10.1146/annurev.pp.31.060180.002423.

Boyd, C.A., Drumheller, S.K., Gates, T.A., 2013. Crocodyliform feeding traces on juvenile ornithischian dinosaurs from the Upper Cretaceous (Campanian) Kaiparowits Formation. Utah. PLoS One 8. https://doi.org/10.1371/journal.pone.0057605.

Brand, W.A., Assonov, S.S., Coplen, T.B., 2010. Correction for the ^{17}O interference in $\delta(^{13}C)$ measurements when analyzing CO_2 with stable isotope mass spectrometry (IUPAC Technical Report). Pure Appl. Chem. 82, 1719–1733. https://doi.org/10.

1351/PAC-REP-09-01-05.
Breecker, D.O., Sharp, Z.D., McFadden, L.D., 2009. Seasonal bias in the formation and stable isotopic composition of pedogenic carbonate in modern soils from central New Mexico, USA. Geol. Soc. Am. Bull. 121, 630–640. https://doi.org/10.1130/B26413.1.
Buck, B.J., Mack, G.H., 1995. Latest Cretaceous (Maastrichtian) aridity indicated by paleosols in the McRae Formation, south-central New Mexico. Cretac. Res. 16, 559–572.
Buol, S., Southard, R., Graham, R., McDaniel, P., 2011. Vertisols: shrinking and swelling dark clay soils. In: Buol, S., Southard, R., Graham, R., McDaniel, P. (Eds.), Soil Genesis and Classification. Wiley-Blackwell, Ames, Iowa.
Burgener, L., Huntington, K.W., Hoke, G.D., Schauer, A., Ringham, M.C., Latorre, C., Díaz, F.P., 2016. Variations in soil carbonate formation and seasonal bias over > 4 km of relief in the western Andes (30°S) revealed by clumped isotope thermometry. Earth Planet. Sci. Lett. 441, 188–199. https://doi.org/10.1016/j.epsl.2016.02.033.
Cermak, V., Bodri, L., Kresl, M., Dedecek, P., Safanda, J., 2016. Eleven years of ground–air temperature tracking over different land cover types. Int. J. Climatol. 37, 1084–1099. https://doi.org/10.1002/joc.4764.
Channan, S., Collins, K., Emanuel, W., 2014. Global Mosaics of the Standard MODIS Land Cover Type Data. College Park, Maryland, USA.
Daëron, M., Blamart, D., Peral, M., Affek, H.P., 2016. Absolute isotopic abundance ratios and the accuracy of Δ_{47} measurements. Chem. Geol. 442, 83–96. https://doi.org/10.1016/j.chemgeo.2016.08.014.
DeConto, R.M., Hay, W.W., Thompson, S.L., Bergengren, J., 1999. Late Cretaceous climate and vegetation interactions: cold continental interior paradox. Spec. Pap. 332. Evol. Cretac. Ocean. Syst. 391–406. https://doi.org/10.1130/0-8137-2332-9.391.
Deconto, R.M., Brady, E.C., Bergengren, J., Hay, W.M., 2000. Late Cretaceous climate, vegetation, and ocean interactions. In: Warm Climates in Earth History, pp. 275–296.
Dee, D.P., Uppala, S.M., Simmons, A.J., Berrisford, P., Poli, P., Kobayashi, S., Andrae, U., Balmaseda, M.A., Balsamo, G., Bauer, P., Bechtold, P., Beljaars, A.C.M., Van De Berg, L., Bidlot, J., Bormann, N., Delsol, C., Dragani, R., Fuentes, M., Geer, A.J., Haimberger, L., Healy, S.B., Hersbach, H., Hólm, E.V., Isaksen, L., Kållberg, P., Köhler, M., Matricardi, M., McNally, A.P., Monge-Sanz, B.M., Morcrette, J.J., Park, B.K., Peubey, C., De Rosnay, P., Tavolato, C., Thépaut, J.N., Vitart, F., 2011. The ERA-Interim reanalysis: configuration and performance of the data assimilation system. Q. J. R. Meteorol. Soc. 137, 553–597.
Dennis, K.J., Affek, H.P., Passey, B.H., Schrag, D.P., Eiler, J.M., 2011. Defining an absolute reference frame for 'clumped' isotope studies of CO2. Geochim. Cosmochim. Acta 75, 7117–7131. https://doi.org/10.1016/j.gca.2011.09.025.
Dennis, K.J., Cochran, J.K., Landman, N.H., Schrag, D.P., 2013. The climate of the Late Cretaceous: new insights from the application of the carbonate clumped isotope thermometer to Western Interior Seaway macrofossil. Earth Planet. Sci. Lett. 362, 51–65. https://doi.org/10.1016/j.epsl.2012.11.036.
Donnadieu, Y., Pierrehumbert, R., Jacob, R., Fluteau, F., 2006. Modelling the primary control of paleogeography on Cretaceous climate. Earth Planet. Sci. Lett. 248, 411–422. https://doi.org/10.1016/j.epsl.2006.06.007.
Driese, S.G., Peppe, D.J., Beverly, E.J., Dipietro, L.M., Arellano, L.N., Lehmann, T., 2016. Paleosols and paleoenvironments of the early Miocene deposits near Karungu, Lake Victoria, Kenya. Palaeogeogr. Palaeoclimatol. Palaeoecol. 443, 167–182. https://doi.org/10.1016/j.palaeo.2015.11.030.
Eiler, J.M., 2007. "Clumped-isotope" geochemistry—the study of naturally-occurring, multiply-substituted isotopologues. Earth Planet. Sci. Lett. 262, 309–327. https://doi.org/10.1016/j.epsl.2007.08.020.
Eiler, J.M., 2011. Paleoclimate reconstruction using carbonate clumped isotope thermometry. Quat. Sci. Rev. 30, 3575–3588. https://doi.org/10.1016/j.quascirev.2011.09.001.
Eiler, J.M., Bergquist, B., Bourg, I., Cartigny, P., Farquhar, J., Gagnon, A., Guo, W., Halevy, I., Hofmann, A., Larson, T.E., Levin, N., Schauble, E.a., Stolper, D., 2014. Frontiers of stable isotope geoscience. Chem. Geol. 372, 119–143. https://doi.org/10.1016/j.chemgeo.2014.02.006.
Falcon-Lang, H.J., 2003. Growth interruptions in silicified conifer woods from the Upper Cretaceous Two Medicine Formation, Montana, USA: Implications for palaeoclimate and dinosaur palaeoecology. Palaeogeogr. Palaeoclimatol. Palaeoecol. 199, 299–314. https://doi.org/10.1016/S0031-0182(03)00539-X.
Farke, A.A., Henn, M.M., Woodward, S.J., Xu, H.A., 2014. *Leidyosuchus* (Crocodylia: Alligatoroidea) from the Upper Cretaceous Kaiparowits Formation (late Campanian) of Utah, USA. PaleoBios 30, 72–88.
Foreman, B.Z., Rogers, R.R., Deino, A.L., Wirth, K.R., Thole, J.T., 2008. Geochemical characterization of bentonite beds in the two Medicine Formation (Campanian, Montana), including a new 40Ar/39Ar age. Cretac. Res. 29, 373–385. https://doi.org/10.1016/j.cretres.2007.07.001.
Foreman, B.Z., Fricke, H.C., Lohmann, K.C., Rogers, R.R., 2011. Reconstructing paleocatchments by integrating stable isotope records, sedimentology, and taphonomy: a Late Cretaceous case study (Montana, United States). PALAIOS 26, 545–554. https://doi.org/10.2110/palo.2010.p10-133r.
Foreman, B.Z., Roberts, E.M., Tapanila, L., Ratigan, D., Sullivan, P., 2015. Stable isotopic insights into paleoclimatic conditions and alluvial depositional processes in the Kaiparowits Formation (Campanian, south-central Utah, U.S.a.). Cretac. Res. 56, 180–192. https://doi.org/10.1016/j.cretres.2015.05.001.
Fricke, H.C., Foreman, B.Z., Sewall, J.O., 2010. Integrated climate model-oxygen isotope evidence for a North American monsoon during the Late Cretaceous. Earth Planet. Sci. Lett. 289, 11–21. https://doi.org/10.1016/j.epsl.2009.10.018.
Friedl, M., Sulla-Menashe, D., Tan, B., Schneider, A., Ramankutty, N., Sibley, A., Huang, X., 2010. MODIS collection 5 global land cover: algorithm refinements and characterization of new datasets, 2001–2012. In: Collection 5.1 IGBP Land Cover. Boston, MA, USA.
Gallagher, T.M., Sheldon, N.D., 2013. A new paleothermometer for forest paleosols and its implications for Cenozoic climate. Geology 41, 647–650. https://doi.org/10.1130/G34074.1.
Gates, T.a., Sampson, S.D., Zanno, L.E., Roberts, E.M., Eaton, J.G., Nydam, R.L., Hutchison, J.H., Smith, J.a., Loewen, M.a., Getty, M.a., 2010. Biogeography of terrestrial and freshwater vertebrates from the late Cretaceous (Campanian) Western Interior of North America. Palaeogeogr. Palaeoclimatol. Palaeoecol. 291, 371–387. https://doi.org/10.1016/j.palaeo.2010.03.008.
Getty, M.A., Loewen, M.A., Roberts, E.M., Titus, A.L., Sampson, S.D., 2010. Taphonomy of horned dinosaurs (Ornithischia: Ceratopsidae) from the late Campanian Kaiparowits Formation, Grand Staircase-Escalante National Monument, Utah. In: Ryan, M., Chinney-Algeier, B., Eberth, D. (Eds.), New Perspectives on Horned Dinosaurs: The Royall Tyrrell Museum Ceratopsian Symposium. Indiana University Press, Bloomington, Indiana.
Ghosh, P., Adkins, J., Affek, H., Balta, B., Guo, W., Schauble, E.a., Schrag, D., Eiler, J.M., 2006. 13C–18O bonds in carbonate minerals: a new kind of paleothermometer. Geochim. Cosmochim. Acta 70, 1439–1456. https://doi.org/10.1016/j.gca.2005.11.014.
Ghosh, P., Vasiliev, M.V., Ghosh, P., Sarkar, S., Ghosh, S., Yamada, K., Ueno, Y., Yoshida, N., Poulsen, C.J., 2016. Tracking the migration of the Indian continent using the carbonate clumped isotope technique on Phanerozoic soil carbonates. Sci. Rep. 6, 1–7. https://doi.org/10.1038/srep22187.
Greenwood, D.R., Wing, S.L., 1995. Eocene continental climates and latitudinal temperature gradients. Geology 23, 1044–1048. https://doi.org/10.1130/0091-7613(1995)023<1044:ECCALT>2.3.CO;2.
Gregory-Wodzicki, K.M., 2000. Relationships between leaf morphology and climate, Bolivia: implications for estimating paleoclimate from fossil floras. Paleobiology 26, 668–688. https://doi.org/10.1666/0094-8373(2000)026<0668:RBLMAC>2.0.CO;2.
Hallam, A., 1984. Continental humid and arid zones during the jurassic and cretaceous. Palaeogeogr. Palaeoclimatol. Palaeoecol. 47, 195–223. https://doi.org/10.1016/0031-0182(84)90094-4.
Hallam, A., 1985. A review of Mesozoic climates. J. Geol. Soc. Lond. 142, 433–445. https://doi.org/10.1144/gsjgs.142.3.0433.
Hay, W.W., 2008. Evolving ideas about the cretaceous climate and ocean circulation. Cretac. Res. 29, 725–753. https://doi.org/10.1016/j.cretres.2008.05.025.
He, B., Olack, G.A., Colman, A.S., 2012. Pressure baseline correction and high-precision CO_2 clumped-isotope (δ 47) measurements in bellows and micro-volume modes. Rapid Commun. Mass Spectrom. 26, 2837–2853. https://doi.org/10.1002/rcm.6436.
Horner, J.R., Schmitt, J.G., Jackson, F., Hanna, R., 2001. Bones and rocks of Upper Cretaceous Two Medicine-Judith River clastic wedge complex, Montana. In: Hill, C. (Ed.), Guidebook for Field Trips: Mesozoic and Cenozoic Paleontology in the Western Plains and Rocky Mountains, Museum of the Rockies Occasional Paper 3. Society of Vertebrate Paleontology, Bozeman, pp. 3–13.
Hough, B.G., Fan, M., Passey, B.H., 2014. Calibration of the clumped isotope geothermometer in soil carbonate in Wyoming and Nebraska, USA: implications for paleoelevation and paleoclimate reconstruction. Earth Planet. Sci. Lett. 391, 110–120. https://doi.org/10.1016/j.epsl.2014.01.008.
Huber, M., 2008. Climate Change. A Hotter Greenhouse? Vol. 321. pp. 353–354.
Huber, M., Caballero, R., 2011. The early Eocene equable climate problem revisited. Clim. Past 7, 603–633. https://doi.org/10.5194/cp-7-603-2011.
Hunter, S.J., Haywood, A.M., Valdes, P.J., Francis, J.E., Pound, M.J., 2013. Modelling equable climates of the Late Cretaceous: can new boundary conditions resolve data-model discrepancies? Palaeogeogr. Palaeoclimatol. Palaeoecol. 392, 41–51. https://doi.org/10.1016/j.palaeo.2013.08.009.
Huntington, K.W., Eiler, J.M., Affek, H.P., Guo, W., Bonifacie, M., Yeung, L.Y., Thiagarajan, N., Passey, B., Tripati, A., Daëron, M., Came, R., 2009. Methods and limitations of "clumped" CO2 isotope (Δ_{47}) analysis by gas-source isotope ratiomass spectrometry. J. Mass Spectrom. 44, 1318–1329. https://doi.org/10.1002/jms.1614.
Hyland, E.G., Sheldon, N.D., Cotton, J.M., 2017. Constraining the early Eocene climatic optimum: a terrestrial interhemispheric comparison. Bull. Geol. Soc. Am. 129, 244–252. https://doi.org/10.1130/B31493.1.
Hyland, E.G., Huntington, K.W., Sheldon, N.D., Reichgelt, T., 2018. Temperature seasonality in the North American continental interior during the Early Eocene Climatic Optimum. Clim. Past. https://doi.org/10.5194/cp-2018-28.
Jordan, G.J., 1997. Uncertainty in palaeoclimatic reconstructions based on leaf physiognomy. Aust. J. Bot. 45, 669–678.
Jordan, G.J., Wing, S.L., Greenwood, D., 1996. Geology Eocene continental climates and latitudinal temperature gradients: comment and reply. Geology 24, 1054. https://doi.org/10.1130/0091-7613(1996)024<1054.
Kauffman, E.G., Caldwell, W.G.E., 1993. The Western Interior Basin in space and time. GAC Spec. Publ. 39, 1–30.
Kelson, J.R., Huntington, K.W., Schauer, A.J., Saenger, C., Lechler, A.R., 2017. Toward a universal carbonate clumped isotope calibration: Diverse synthesis and preparatory methods suggest a single temperature relationship. Geochim. Cosmochim. Acta 197, 104–131. https://doi.org/10.1016/j.gca.2016.10.010.
Kelson, J.R., Watford, D., Bataille, C., Huntington, K.W., Hyland, E., Bowen, G.J., 2018. Warm terrestrial subtropics during the Paleocene and Eocene: carbonate clumped isotope (Δ_{47}) evidence from the Tornillo Basin, Texas (USA). Paleoceanogr. Paleoclimatology 33, 1–20. https://doi.org/10.1029/2018PA003391.
Kowalski, E. a, Dilcher, D.L., 2003. Warmer paleotemperatures for terrestrial ecosystems. Proc. Natl. Acad. Sci. U. S. A. 100, 167–170. https://doi.org/10.1073/pnas.232693599.
Kump, L.R., Slingerland, R.L., 1999. Circulation and stratification of the early Turonian Western Interior Seaway: sensitivity to a variety of forcings. In: Special Paper 332: Evolution of the Cretaceous Ocean–Climate System, pp. 181–190. https://doi.org/10.1130/0-8137-2332-9.181.
Lehman, T.M., 2001. Late Cretaceous dinosaur provinciality. In: Tanke, D., Carpenter, K.

(Eds.), Mesozoic Vertebrate Life. Indiana University Press, Bloomington, pp. 310–328.
Lehman, T.M., McDowell, F.W., Connelly, J.N., 2006. First isotopic (U-Pb) age for the Late Cretaceous *Alamosaurus* vertebrate fauna of west Texas, and its significance as a link between two faunal provinces. J. Vertebr. Paleontol. 26, 922–928. https://doi.org/10.1671/0272-4634(2006)26.
Leslie, C.E., Peppe, D.J., Williamson, T.E., Heizler, M., Jackson, M., Atchley, S.C., Nordt, L., Standhardt, B., 2018. Revised Age Constraints for Late Cretaceous to Early Paleocene Terrestrial Strata From the Dawson Creek Section, Big Bend National Park, West Texas. pp. 1–21.
Lozinsky, R., Hunt, A., Wolberg, D., Lucas, S., 1984. Late Cretaceous (Lancian) dinosaurs from the McRae Formation, Sierra County, New Mexico. N. M. Geol. 6, 72–77.
Lucas, S.G., Sullivan, R.M., Lichtig, A.J., Dalman, S.G., Jasinski, S.E., 2016. Late Cretaceous dinosaur biogeography and endemism in the Western Interior basin, North America: a critical re-evaluation. New Mex. Museum Nat. Hist. Sci. Bull. 71, 195–213.
Mack, G.H., James, W.C., Monger, H.C., 1993. Classification of paleosols. Geol. Soc. Am. Bull. 105, 129–136. https://doi.org/10.1130/0016-7606(1993)105<0129.
Markwick, P.J., 1998. Fossil crocodilians as indicators of late cretaceous and Cenozoic climates: Implications for using palaeontological data in reconstructing palaeoclimate. Palaeogeogr. Palaeoclimatol. Palaeoecol. 137, 205–271. https://doi.org/10.1016/S0031-0182(97)00108-9.
Matthews, H.D., Eby, M., Ewen, T., Friedlingstein, P., Hawkins, B.J., 2007. What determines the magnitude of carbon cycle-climate feedbacks? Glob. Biogeochem. Cycles 21, 1–12. https://doi.org/10.1029/2006GB002733.
Maynard, J.B., 1992. Chemistry of modern soils as a guide to interpreting Precambrian paleosols. J. Geol. 100, 279–289. https://doi.org/10.1086/629632.
Meckler, A.N., Ziegler, M., Millán, M.I., Breitenbach, S.F.M., Bernasconi, S.M., 2014. Long-term performance of the Kiel carbonate device with a new correction scheme for clumped isotope measurements. Rapid Commun. Mass Spectrom. 28, 1705–1715. https://doi.org/10.1002/rcm.6949.
Miller, I.M., Johnson, K.R., Kline, D.E., Nichols, D.J., Barclay, R.S., 2013. A Late Campanian flora from the Kaiparowits Formation, Southern Utah, and a brief overview of the widely sampled but little-known Campanian vegetation of the Western Interior of North America. In: Titus, A.L., Loewen, M.A. (Eds.), At the Top of the Grand Staircase. Indiana University Press, Bloomington, Indiana, pp. 107–131.
Morrone, J.J., 2014. Parsimony analysis of endemicity (PAE) revisited. J. Biogeogr. 41, 842–854. https://doi.org/10.1111/jbi.12251.
Niezgodzki, I., Knorr, G., Lohmann, G., Tyszka, J., Markwick, P.J., 2017. Late Cretaceous climate simulations with different CO_2 levels and subarctic gateway configurations: a model-data comparison. Paleoceanography 32, 980–998. https://doi.org/10.1002/2016PA003055.
Nordt, L.C., Driese, S.G., 2010. A Modern soil characterization approach to reconstructing physical and chemical properties of paleo-vertisols. Am. J. Sci. 310, 37–64. https://doi.org/10.2475/01.2010.02.
Nordt, L., Atchley, S., Dworkin, S., 2003. Terrestrial evidence for two greenhouse events in the latest Cretaceous. GSA Today 13, 4–9. https://doi.org/10.1130/1052-5173(2003)013<4:TEFTGE>2.0.CO;2.
Nordt, L., Orosz, M., Driese, S., Tubbs, J., 2006. Vertisol carbonate properties in relation to mean annual precipitation: implications for paleoprecipitation estimates. J. Geol. 114, 501–510. https://doi.org/10.1086/504182.
Nordt, L.C., Dworkin, S.I., Atchley, S.C., 2011. Ecosystem response to soil biogeochemical behavior during the Late Cretaceous and early Paleocene within the western interior of North America. Geol. Soc. Am. Bull. 123, 1745–1762. https://doi.org/10.1130/B30365.1.
Nydam, R.L., Rowe, T.B., Cifelli, R.L., 2013. Lizards and snakes of the Terlingua Local Fauna (late Campanian), Aguja Formation, Texas, with comments on the distribution of paracontemporaneous squamates throughout the Western Interior of North America. J. Vertebr. Paleontol. 33, 1081–1099. https://doi.org/10.1080/02724634.2013.760467.
Parker, A., 1970. Index of weathering for silicate rocks. Geol. Mag. 107, 501–504.
Parrish, J.T., Ziegler, A.M., Scotese, C.R., 1982. Rainfall patterns and the distribution of coals and evaporites in the Mesozoic and Cenozoic. Palaeogeogr. Palaeoclimatol. Palaeoecol. 40, 67–101. https://doi.org/10.1016/0031-0182(82)90085-2.
Passey, B.H., Levin, N.E., Cerling, T.E., Brown, F.H., Eiler, J.M., 2010. High-temperature environments of human evolution in East Africa based on bond ordering in paleosol carbonates. Proc. Natl. Acad. Sci. 107, 11245–11249. https://doi.org/10.1073/pnas.1001824107.
Peppe, D.J., Royer, D.L., Wilf, P., Kowalski, E.A., 2010. Quantification of large uncertainties in fossil leaf paleoaltimetry. Tectonics 29. https://doi.org/10.1029/2009TC002549.
Peppe, D.J., Royer, D.L., Cariglino, B., Oliver, S.Y., Newman, S., Leight, E., Enikolopov, G., Fernandez-Burgos, M., Herrera, F., Adams, J.M., Correa, E., Currano, E.D., Erickson, J.M., Hinojosa, L.F., Hoganson, J.W., Iglesias, A., Jaramillo, C.a., Johnson, K.R., Jordan, G.J., Kraft, N.J.B., Lovelock, E.C., Lusk, C.H., Niinemets, Ü., Peñuelas, J., Rapson, G., Wing, S.L., Wright, I.J., 2011. Sensitivity of leaf size and shape to climate: global patterns and paleoclimatic applications. New Phytol. 190, 724–739. https://doi.org/10.1111/j.1469-8137.2010.03615.x.
Peppe, D.J., Baumgartner, A., Flynn, A., Blonder, B., 2017. Reconstructing paleoclimate and paleoecology using fossil leaves. PaleorXiv Pap. 1–78. https://doi.org/10.31233/osf.io/stzuc.
Peters, N.a., Huntington, K.W., Hoke, G.D., 2013. Hot or not? Impact of seasonally variable soil carbonate formation on paleotemperature and O-isotope records from clumped isotope thermometry. Earth Planet. Sci. Lett. 361, 208–218. https://doi.org/10.1016/j.epsl.2012.10.024.
Poulsen, C.J., Barron, E.J., Johnson, C.C., Fawcett, P., 1999. Links between major climatic factors and regional oceanic circulation in the mid-Cretaceous. In: Evolution of the Cretaceous Ocean–Climate System, Special Paper Geological Society of America, pp. 73–90. https://doi.org/10.1130/0-8137-2332-9.73.
Poulsen, C.J., Pollard, D., White, T.S., 2007. General circulation model simulation of the $\delta^{18}O$ content of continental precipitation in the middle Cretaceous: a model-proxy comparison. Geology 35, 199–202. https://doi.org/10.1130/G23343A.1.
Quade, J., Garzione, C., Eiler, J., 2007. Paleoelevation reconstruction using pedogenic carbonates. Rev. Mineral. Geochem. 66, 53–87. https://doi.org/10.2138/rmg.2007.66.3.
Quade, J., Eiler, J., Daëron, M., Achyuthan, H., 2013. The clumped isotope geothermometer in soil and paleosol carbonate. Geochim. Cosmochim. Acta 105, 92–107. https://doi.org/10.1016/j.gca.2012.11.031.
Reichgelt, T., West, C.K., Greenwood, D.R., 2018. The relation between global palm distribution and climate. Sci. Rep. 8, 2–12. https://doi.org/10.1038/s41598-018-23147-2.
Retallack, G.J., 1994. A pedotype approach to latest Cretaceous and earliest tertiary paleosols in eastern Montana. Geol. Soc. Am. Bull. 106, 1377–1397. https://doi.org/10.1130/0016-7606(1994)106<1377:APATLC>2.3.CO;2.
Retallack, G.J., 2005. Pedogenic carbonate proxies for amount and seasonality of precipitation in paleosols. Geology 33, 333. https://doi.org/10.1130/G21263.1.
Retallack, G.J., James, W.C., Mack, G.H., Monger, H.C., 1993. Geological Society of America Bulletin Classification of paleosols: discussion and reply. Geol. Soc. Am. Bull. https://doi.org/10.1130/0016-7606(1993)105<1635.
Ringham, M.C., Hoke, G.D., Huntington, K.W., Aranibar, J.N., 2016. Influence of vegetation type and site-to-site variability on soil carbonate clumped isotope records, Andean piedmont of Central Argentina (32-34??S). Earth Planet. Sci. Lett. 440, 1–11. https://doi.org/10.1016/j.epsl.2016.02.003.
Roberts, E.M., 2005. Stratigraphic, Taphonomic, and Paleoenvironmental Analysis of the Upper Cretaceous Kaiparowits Formation, Grand Staircase-Escalante National Monument, Souther Utah. University of Utahhttps://doi.org/10.1177/001088048102200214.
Roberts, E.M., 2007. Facies architecture and depositional environments of the Upper Cretaceous Kaiparowits Formation, southern Utah. Sediment. Geol. 197, 207–233. https://doi.org/10.1016/j.sedgeo.2006.10.001.
Roberts, L.N.R., Kirschbaum, M.A., 1995. Paleogeography of the Late Cretaceous of the western interior of middle North America—coal distribution and sediment accumulation. Washington DC. In: U.S. Geological Survey Profesional Paper 1561.
Roberts, E.M., Deino, A.L., Chan, M.a., 2005. 40Ar/39Ar age of the Kaiparowits Formation, southern Utah, and correlation of contemporaneous Campanian strata and vertebrate faunas along the margin of the Western Interior Basin. Cretac. Res. 26, 307–318. https://doi.org/10.1016/j.cretres.2005.01.002.
Rogers, R.R., 1995. Sequence Stratigraphy and Vertebrate Taphonomy of the Upper Cretaceous Two Medicine and Judith River Formations, Montana. https://doi.org/10.16953/deusbed.74839.
Rogers, R.R., 1998. Sequence analysis of the Upper Cretaceous Two Medicine and Judith River formations, Montana; nonmarine response to the Claggett and Bearpaw marine cycles. J. Sediment. Res. 68, 615–631. https://doi.org/10.2110/jsr.68.604.
Rogers, R.R., Swisher III, C.C., Horner, J.R., 1993. 40Ar/39Ar age and correlation of the nonmarine Two Medicine Formation (Upper Cretaceous), northwestern Montana, U.S.A. Can. J. Earth Sci. 30, 1066–1075. https://doi.org/10.1139/e93-090.
Ross, S.M., 2003. Peirce's criterion for the elimination of suspect experimental data. J. Eng. Technol. 20, 1–12.
Royer, D.L., 2012. Climate reconstruction from leaf size and shape: new developments and challenges. Paleontol. Soc. Pap. 18, 195–212.
Sampson, S.D., Loewen, M.A., Farke, A.A., Roberts, E.M., Forster, C.A., Smith, J.A., Titus, A.L., 2010. New horned dinosaurs from Utah provide evidence for intracontinental dinosaur endemism. PLoS One 5, 1–12. https://doi.org/10.1371/journal.pone.0012292.
Schatz, A.K., Scholten, T., Kühn, P., 2015. Paleoclimate and weathering of the Tokaj (Hungary) loess-paleosol sequence. Palaeogeogr. Palaeoclimatol. Palaeoecol. 426, 170–182. https://doi.org/10.1016/j.palaeo.2015.03.016.
Schauer, A.J., Kelson, J., Saenger, C., Huntington, K.W., 2016. Choice of 17O correction affects clumped isotope (Δ_{47}) values of CO2 measured with mass spectrometry. Rapid Commun. Mass Spectrom. 30, 2607–2616. https://doi.org/10.1002/rcm.7743.
Sewall, J.O., Fricke, H.C., 2013. Andean-scale highlands in the late cretaceous Cordillera of the north American western margin. Earth Planet. Sci. Lett. 362, 88–98. https://doi.org/10.1016/j.epsl.2012.12.002.
Sewall, J.O., Sloan, L.C., 2006. Come a little bit closer: a high-resolution climate study of the early Paleogene Laramide foreland. Geology 34, 81–84. https://doi.org/10.1130/G22177.1.
Sharkey, T.D., 2000. Some like it hot. Science 287, 435.
Sheldon, N.D., Tabor, N.J., 2009. Quantitative paleoenvironmental and paleoclimatic reconstruction using paleosols. Earth Sci. Rev. 95, 1–52. https://doi.org/10.1016/j.earscirev.2009.03.004.
Sheldon, N.D., Retallack, G.J., Tanaka, S., 2002. Geochemical Climofunctions from North American soils and application to paleosols across the Eocene-Oligocene boundary in Oregon. J. Geol. 110, 687–696. https://doi.org/10.1086/342865.
Sloan, L.C., Barron, E.J., 1990. “Equable” climates during Earth history? Geology 18, 489–492. https://doi.org/10.1130/0091-7613(1990)018<0489:ECDEH>2.3.CO;2.
Sloan, L.C., Morrill, C., 1998. Orbital forcing and Eocene continental temperatures. Palaeogeogr. Palaeoclimatol. Palaeoecol. 144, 21–35. https://doi.org/10.1016/S0031-0182(98)00091-1.
Smith, S.Y., Manchester, S.R., Samant, B., Dhananjay, M., Wheeler, E., Baas, P., Kapgate, D., Sheldon, N.D., 2015. Integrating paleobotanical, paleosol, and stratigraphic data to study critical transitions: a case study from the Late Cretaceous – Paleocene of India. Earth-Life Transitions Paleobiol. Context Earth Syst. Evol. Paleontol. Soc. Pap.

21. https://doi.org/10.1039/C4RA16014B.
Snell, K.E., Thrasher, B.L., Eiler, J.M., Koch, P.L., Sloan, L.C., Tabor, N.J., 2013. Hot summers in the Bighorn Basin during the early Paleogene. Geology 41, 55–58. https://doi.org/10.1130/G33567.1.
Snell, K.E., Koch, P.L., Druschke, P., Foreman, B.Z., Eiler, J.M., 2014. High elevation of the “Nevadaplano” during the Late Cretaceous. Earth Planet. Sci. Lett. 386, 52–63. https://doi.org/10.1016/j.epsl.2013.10.046.
Spicer, R.A., Yang, J., 2010. Quantification of uncertainties in fossil leaf paleoaltimetry: does leaf size matter? Tectonics 29, 1–13. https://doi.org/10.1029/2010TC002741.
Spicer, R.A., Herman, A.B., Kennedy, E.M., 2004. Foliar physiognomic record of climatic conditions during dormancy: climate leaf analysis multivariate program (CLAMP) and the cold month mean temperature. J. Geol. 112, 685–702. https://doi.org/10.1086/424579.
Spicer, R.A., Herman, A.B., Kennedy, E.M., 2005. The sensitivity of CLAMP to taphonomic loss of foliar physiognomic characters. PALAIOS 20, 429–438. https://doi.org/10.2110/palo.2004.P04-63.
Spicer, R.A., Ahlberg, A., Herman, A.B., Hofmann, C.C., Raikevich, M., Valdes, P.J., Markwick, P.J., 2008. The Late Cretaceous continental interior of Siberia: a challenge for climate models. Earth Planet. Sci. Lett. 267, 228–235. https://doi.org/10.1016/j.epsl.2007.11.049.
Spicer, R.A., Bera, S., De Bera, S., Spicer, T.E.V., Srivastava, G., Mehrotra, R., Mehrotra, N., Yang, J., 2011. Why do foliar physiognomic climate estimates sometimes differ from those observed? Insights from taphonomic information loss and a CLAMP case study from the Ganges Delta. Palaeogeogr. Palaeoclimatol. Palaeoecol. 302, 381–395. https://doi.org/10.1016/j.palaeo.2011.01.024.
Stinchcomb, G.E., Nordt, L.C., Driese, S.G., Lukens, W.E., Williamson, F.C., Tubbs, J.D., 2016. A data-driven spline model designed to predict paleoclimate using paleosol geochemistry. Am. J. Sci. https://doi.org/10.2475/08.2016.02.
Suarez, M.B., Passey, B.H., Kaakinen, A., 2011. Paleosol carbonate multiple isotopologue signature of active east Asian summer monsoons during the late Miocene and Pliocene. Geology 39, 1151–1154. https://doi.org/10.1130/G32350.1.
Suarez, M.B., Ludvigson, G.A., Gonzalez, L.A., You, H.L., 2017. Continental paleotemperatures from an early cretaceous Dolomitic Lake, Gansu Province, China. J. Sediment. Res. 486–499. https://doi.org/10.2110/jsr.2017.31.
Thrasher, B.L., Sloan, L.C., 2010. Land cover influences on the regional climate of western North America during the early Eocene. Glob. Planet. Change 72, 25–31. https://doi.org/10.1016/j.gloplacha.2010.02.002.
Tidwell, W.D., Britt, B.B., Tidwell, L.S., 2007. A review of the Cretaceous floras of east-central Utah and western Colorado. In: Central Utah: Diverse Geology of a Dynamic Landscape, UGA Publication 36. Utah Geological Association publication, pp. 466–481.
Upchurch, G.R., Kiehl, J., Shields, C., Scherer, J., Scotese, C., 2015. Latitudinal temperature gradients and high-latitude temperatures during the latest Cretaceous: congruence of geologic data and climate models. Geology 43, 683–686. https://doi.org/10.1130/G36802.1.
Valdes, P., 2011. Built for stability. Nat. Geosci. 4, 414–416. https://doi.org/10.1038/ngeo1200.
Van Boskirk, C.M., 1998. The Flora of the Eagle Formation and Its Significance for Late Cretaceous Floristic Evolution. Yale University.
Varricchio, D.J., 1995. Taphonomy of Jack's Birthday Site, a diverse dinosaur bonebed from the Upper Cretaceous Two Medicine Formation of Montana. Palaeogeogr. Palaeoclimatol. Palaeoecol. 114, 297–323. https://doi.org/10.1016/0031-0182(94)00084-L.
Wolfe, J.A., 1990. Paleobotantical evidence for a major temperature increase following the Cretaceous/Tertiary boundary. Nature 343, 153–156.
Wolfe, J.A., Upchurch, G.R., 1987. North American nonmarine climates and vegetation during the late cretaceous. Palaeogeogr. Palaeoclimatol. Palaeoecol. 61, 33–77. https://doi.org/10.1016/0031-0182(87)90040-X.
Zaarur, S., Affek, H.P., Brandon, M.T., 2013. A revised calibration of the clumped isotope thermometer. Earth Planet. Sci. Lett. 382, 47–57. https://doi.org/10.1016/j.epsl.2013.07.026.